

1 **Sea-level variability and change along the Norwegian coast between 2003** 2 **and 2018 from satellite altimetry, tide gauges and hydrography**

3 Fabio Mangini¹, Léon Chafik^{2,3}, Antonio Bonaduce¹, Laurent Bertino¹, Jan Even Ø. Nilsen⁴

4 ¹Nansen Environmental and Remote Sensing Center and Bjerknes Centre for Climate Research, Bergen, Norway

5 ²Department of Meteorology and Bolin Centre for Climate Research, Stockholm, Sweden

6 ³National Oceanography Centre, Southampton, UK

7 ⁴Institute of Marine Research and Bjerknes Centre for Climate Research, Bergen, Norway

8 *Correspondence to:* Fabio Mangini (fabio.mangini@nerisc.no)

9 **Abstract.** Sea-level variations in coastal areas can differ significantly from those in the nearby open ocean.
10 Monitoring coastal sea-level variations is therefore crucial to understand how climate variability can affect the
11 densely populated coastal regions of the globe. In this paper, we study the sea-level variability along the coast
12 of Norway by means of in situ records, satellite altimetry data, and a network of eight hydrographic stations
13 over a period spanning 16 years (from 2003 to 2018). At first, we evaluate the performance of the ALES-
14 reprocessed coastal altimetry dataset (1 Hz posting rate) by comparing it with the sea-level anomaly from tide
15 gauges over a range of timescales, which include the long-term trend, the annual cycle and the detrended and
16 deseasoned sea-level anomaly. We find that coastal altimetry and conventional altimetry products performs
17 similarly along the Norwegian coast. However, the agreement with tide-gauges in terms of trends ~~are~~ is on
18 average ~~10%~~ 6% better when we use the ALES coastal altimetry data. We later assess the steric contribution to
19 the sea-level along the Norwegian coast. While longer time series are necessary to evaluate the steric
20 contribution to the sea-level trends, we find that the sea-level annual cycle is more affected by variations in
21 temperature than in salinity, and that both temperature and salinity give a comparable contribution to the
22 detrended and deseasoned sea-level ~~change~~ variability along the entire Norwegian coast. A conclusion from our
23 study is that coastal regions poorly covered by tide gauges can benefit from our satellite-based approach to
24 study and monitor sea-level change and variability.

25 1 Introduction

26 ~~Sea level is considered a key indicator to monitor the earth's energy imbalance and climate change (e.g.,~~
27 ~~Oppenheimer et al., 2019; von Schuckmann et al., 2018). An accurate estimate and attribution~~ Global mean sea
28 level (GMSL) has been rising during the XX century and the beginning of the XXI century at a rate of
29 approximately 1.5 mm year⁻¹ (Frederikse et al., 2020). Its rise is projected to continue, and even accelerate, in
30 the future (Hermans et al., 2021), thus posing significant stress on coastal communities (Nicholls, 2011). At a
31 local scale, though, sea-level variations can largely depart from the global average (Stammer et al., 2013).
32 Therefore, an accurate estimation and attribution of sea-level rise at regional scale is one of the major
33 challenges of climate research (Frederikse et al., 2018), with large societal benefit and impact due to the large
34 human population living in coastal areas (e.g., Lichter et al., 2011). The Norwegian coast is no exception. While
35 it appears little vulnerable to sea-level variations because of its steep topography and rocks resistant to erosion,
36 it has a large number of coastal cities, most of which have undergone significant urban development in recent
37 times (Simpson et al., 2015).

38

39 Since August 1992, when NASA and CNES launched the TOPEX/Poseidon mission, satellite altimetry has
40 enormously expanded our knowledge of the ocean and the climate system (e.g., Cazenave et al., 2018). With
41 the help of satellite altimetry, oceanographers and climate scientists could observe sea-level variations over
42 almost the entire ocean (e.g., Nerem et al., 2010; Madsen et al., 2019) and understand their causes (e.g.,
43 Richter et al., 2020), detect ocean currents (e.g., Zhang et al., 2007) and monitor their variability (e.g., Chafik et
44 al., 2015), observe the evolution of climate events (e.g., Ji et al., 2000) and investigate their origins (e.g., Picaut
45 et al., 2002). Satellite altimetry has made these, and other achievements, possible because it has provided
46 continuous sea-level observations over large parts of the ocean, in areas where sea-level measurements were
47 previously only occasional.

48

49 While invaluable over the open ocean, satellite altimetry measurements have historically been flagged as
50 unreliable in coastal areas (e.g., Benveniste et al., 2020). Indeed, the accuracy of radar altimetry, which is 2-3
51 cm over the open ocean (e.g., Volkov and Pujol, 2012), deteriorates in coastal regions because of technical
52 issues (e.g., Xu et al., 2019). Notably, large variations in the backscattering of the area illuminated by the radar

53 altimeters (for example, due to the presence of land or to patches of very calm water in sheltered areas;
54 Gómez-Enri et al., 2010) contaminate the returned echoes of radar altimeters, and the complex topography of
55 continental shelves, together with the irregular shape of most coastlines, makes geophysical corrections in
56 coastal areas less accurate than in the open ocean.

57

58 To increase the accuracy of radar altimetry in coastal regions, Passaro et al. (2014) have developed the Adaptive
59 Leading Edge Subwaveform (ALES) retracking algorithm. The ALES retracker addresses the altimeter footprint
60 contamination issue by avoiding echoes from bright targets (e.g., land). Several studies have found a clear
61 improvement of the ALES-reprocessed satellite altimetry observations over conventional altimetry products in
62 different areas of the World (e.g., Passaro et al., 2014, 2015, 2016, 2018, 2021), with the new algorithm
63 providing estimates of the altimetry parameters in coastal areas with levels of accuracy typical of the open
64 ocean for distances to the coast of up to 3 km circa (e.g., Passaro et al., 2014).

65

66 In this paper, we investigate how the ALES-reprocessed satellite altimetry dataset resolves sea-level along the
67 coast of Norway compared to all the tide-gauge records available over the 16-year period between 2003 and
68 2018. Indeed, to the best of our knowledge, previous validation studies have not considered the entire
69 Norwegian coast, but only parts of it: Passaro et al. (2015) focused on the transition zone between the North
70 Sea and the Baltic Sea, whereas Rose et al. (2019) focused on Honningsvåg, in northern Norway. The Norwegian
71 coast also appears particularly interesting for validation purposes because, during the altimetry period, it is well
72 covered by tide gauges, and because conventional altimetry products have previously failed to reproduce the
73 sea-level trends in the region (Breili et al., 2017). The present study will thus investigate the performance of
74 ALES in relation to these issues.

75

76 We further use the ALES-reprocessed altimetry dataset in combination with a network of hydrographic stations
77 along the coast of Norway to study the steric contribution to the sea-level variability in the region ~~the local sea-~~
78 ~~level budget~~, which is known to be challenging at the regional scale (e.g., Raj et al., 2020; Richter et al., 2012).
79 Richter et al. (2012) have already used tide gauges and hydrographic stations to assess the different
80 contributions to the Norwegian sea-level variability between 1960 and 2010. However, compared to their study,
81 we use the coastal altimetry dataset to reconstruct a monthly mean sea-level time series centred over each

82 hydrographic station. This is an advantage over Richter et al. (2012) since some of the Norwegian tide gauges
83 are located in sheltered areas and might not be representative of the variability captured by the nearest
84 hydrographic station (which can be as far as 100 km apart). Moreover, compared to Richter et al. (2012), we
85 analyse the annual cycle of the sea-level more in detail by describing how its properties change along the
86 Norwegian coast. Furthermore, sea-level measurements from satellite altimetry, unlike those from tide gauges,
87 do not need to be corrected for vertical land motion.

88

89 This paper is organized as follows. Section 2 describes the data used in the coastal sea-level signal analysis. An
90 analysis of sea-level components retrieved by each observational instrument is provided in Section 3. The
91 coastal sea level from tide gauges and satellite altimetry are compared in terms of temporal variability and
92 trends in Section 4. Section 5 focuses on the steric contribution to the sea-level estimates from altimetry, tide
93 gauges, and hydrographic data. Section 6 summarizes and concludes.

94

95 **2 Data**

96 **2.1 ALES-reprocessed multi-mission satellite altimetry**

97 To provide more accurate sea-level estimates in coastal regions, the ALES retracker operates in two stages. At
98 first, it fits the leading edge of the waveform to have a rough estimate of the significant wave height (SWH).
99 Then, depending on the SWH, the algorithm selects a portion of the waveform (known as subwaveform) and fits
100 it to estimate the range (the distance between the satellite and the sea surface), the SWH and the backscatter
101 coefficient.

102

103 The dataset is freely available at the Open Altimetry Database website of the Technische Universität München
104 (<https://openadb.dgfi.tum.de/en/>). The European Space Agency (ESA) also provides, through The Sea Level
105 Climate Change Initiative Programme, a coastal satellite altimetry dataset reprocessed with the ALES-retracker.
106 However, it only covers the northern latitudes up to 60°N and, therefore, only part of the region of interest in
107 this study (Benveniste et al., 2020).

108

109 The dataset ~~and~~ includes observations from the following altimetry missions: Envisat (version 3), Jason-1, Jason-
110 1 extended mission, Jason-1 geodetic mission, Jason-2, Jason-2 extended mission, Jason 3, SARAL, SARAL
111 drifting phase, ~~Sentinel-3A and Sentinel-3B~~. These are provided at a 1 Hz posting rate (equivalent to an along-
112 track resolution of circa 7 km) and cover the period from June 2002 to April 2020, with the exception of one
113 data gap between November 2010 (end of Envisat) and March 2013 (start of SARAL) to the north of 66° N. Data
114 from different missions have been cross-calibrated, so that there are no inter-mission biases.

115

116 Prior to distribution, several corrections have been applied to the satellite altimetry data. Among them, ~~all the~~
117 ~~corrections applied to the altimetry data~~ the geophysical corrections are of particular interest for the purpose of
118 this study. Indeed, to validate the ALES-reprocessed altimetry against the Norwegian tide gauges, the same
119 physical signal must be removed from both datasets. The geophysical corrections applied to the ALES-
120 reprocessed altimetry data include the tidal and the dynamic atmospheric corrections (COSTA user manual,
121 [http://epic.awi.de/43972/1/User Manual COSTA v1 0.pdf](http://epic.awi.de/43972/1/User_Manual_COSTA_v1_0.pdf)). ~~The tidal correction include the is performed~~
122 ~~using the EOT11a tidal model~~. The correction for ocean and pole tides has been performed using the EOT11a
123 tidal model. The solid Earth related tides have also been subtracted from the orbital altitude but, as it leaves the
124 altimetry data in sync with the tide gauges (which are based on the solid Earth), this correction has no further
125 interest for this study. The dynamic atmospheric correction (DAC), available at
126 <https://www.aviso.altimetry.fr/index.php?id=1278>, removes both the wind and the pressure contribution to
127 the sea-level variability at timescales shorter than 20 days, and only the pressure contribution to the sea-level
128 variability at longer timescales. The high-frequency component of the DAC is computed using the Mog2D-G
129 High Resolution barotropic model (Carrère and Lyard, 2003), and it is removed because it would otherwise alias
130 the altimetry data. The low-frequency component accounts for the static response of the sea-level to changes in
131 pressure, a phenomenon also known as inverse barometer effect (IBE), and according to which a 1 hPa
132 increase/decrease in sea-level pressure corresponds to a 1 cm decrease/increase in sea-level. To validate the
133 ALES-reprocessed altimetry against the Norwegian tide gauges, the relevant physical signals at the relevant time
134 scales must be removed from the tide gauge data (Section 2.2).

135

136

137 The producers of ALES flag some of the data as unreliable. More precisely, they recommend excluding
138 observations that fall within a distance of 3 km from the coast and whose sea-level anomaly (SLA), SWH, and
139 standard deviation exceed 2.5 m, 11 m, and 0.2 m respectively. We have followed these recommendations with
140 one exception: we have lowered the threshold on the sea-level anomaly from 2.5 to 1.5 m because this choice
141 leads to a better agreement between the tide gauges and the ALES altimetry dataset between Måløy and
142 Rørvik, along the west coast of Norway (Fig. 1).

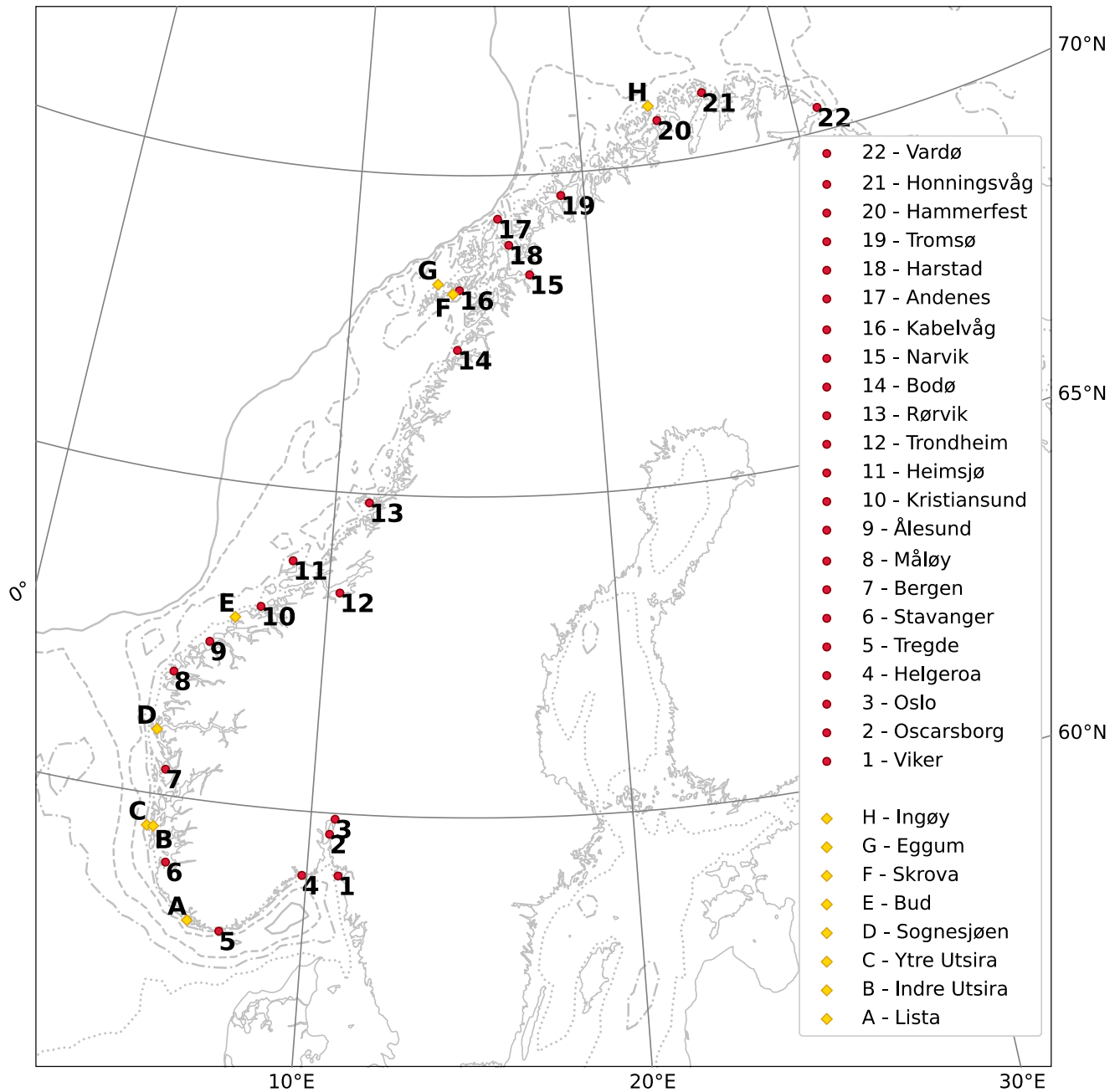
143 **2.2 Tide gauges**

144 The Norwegian Mapping Authority (Kartverket) provides information on observed water levels at 24 permanent
145 tide gauge stations along the coast of Norway. Data are updated, referenced to a common datum, quality
146 checked, and freely distributed through a dedicated web API (api.sehavniva.no).

147
148 Even though most tide gauges provide a few decades of sea-level measurements, in this study we only consider
149 the period between January 2003 and December 2018 because it overlaps with the time-window spanned by
150 the ALES-altimetry dataset. Moreover, we only select 22 of the 24 permanent tide gauges available: we exclude
151 Mausund, since it has no measurements available before November 2010, and Ny-Ålesund, because it is outside
152 of our region of interest.

153
154 Over the period considered, the only tide gauges with missing values are Heimsjø and Hammerfest, with a 1-
155 month gap, and Oslo, with a 2-month gap. We expect the Norwegian set of tide gauges to map the coastal sea-
156 level with a spatial resolution of circa 130 km as it corresponds to the mean distance between adjacent tide
157 gauges. This estimate should be treated only as a first order approximation of the spatial resolution since the
158 distance between adjacent tide gauges varies along the Norwegian coast and ranges from ~30 km, in southern
159 Norway, to ~300 km, in western Norway (more precisely, between Rørvik and Bodø).

160



161
 162 Figure 1: Location of the tide gauges and of the hydrographic stations considered in this study (red circles and yellow diamonds
 163 respectively). The solid, dashed, dash-dotted and dotted light gray lines indicate the 500 m, 300 m, 150 m, and 50 m isobaths,
 164 respectively.

165

166 A number of geophysical corrections have been applied to the tide gauge data for them to be consistent with
167 the sea-level anomaly from altimetry. These include the effects of the glacial isostatic adjustment (GIA), the
168 ~~nodal~~ low frequency tides, and the DAC.

169
170 The GIA results from the adjustment of the earth to the melting of the Fennoscandian ice sheet since the last
171 glacial maximum, circa 20 thousand years ago. The earth's relaxation affects substantially the sea-level change
172 relative to the Norwegian coast, with values ranging from approximately 1 up to 5 mm year⁻¹ (e.g., Breili et al.,
173 2017). Along the Norwegian coast, the GIA affects the sea-level reading from the tide gauges because it
174 induces a vertical land movement (VLM) and, to a lesser extent the sea level itself, because it modifies the
175 earth's gravity field. The first effect has been corrected using both GNSS observations and levelling, whereas the
176 second has not been corrected ~~using a GIA model~~ since the satellite altimetry data are also influenced by geoid
177 changes (Simpson et al., 2017).

178
179 The low frequency constituents of ocean tide, derived from the EOT11a tidal model, are removed from the tide
180 gauge data as they are from the ALES-reprocessed altimetry dataset. Hammerfest, Honningsvåg and Vardø, the
181 three northernmost tide gauges (Fig. 1), are located outside of the EOT11a model domain. Therefore, at these
182 three locations, we remove the low frequency constituents of ocean tide for Tromsø. The constituents in
183 question are the solar semiannual, solar annual, and the nodal tide. For Norway the solar annual astronomical
184 tide is negligible, while the two latter constituents have amplitudes on the order of 1 cm. The nodal tide has a
185 period of approximately 18.61 years and results from the precession of the lunar nodes around the ecliptic
186 (Woodworth, 2012). As our time series are shorter than the nodal cycle, this constituent is not negligible with
187 regards to our trend analysis. None of the solid earth related tides needs to be removed from land-locked tide
188 gauge measurements to produce sea-level records comparable to altimetric sea surface height. Moreover, the
189 ocean pole tide, not provided by the EOT11a, has not been removed from the tide gauge data. However, it is
190 negligible in our region.

191
192 Since we have provided a description of the DAC in the previous section, here we only briefly describe how we
193 have applied it to the tide gauge data. At first, we have monthly averaged the six hourly DAC dataset (available
194 at the AVISO+ website, <https://www.avis0.altimetry.fr/en/data/products/auxiliary-products/dynamic->

195 [atmospheric-correction.html](#)). Then, for each tide gauge, we have computed the difference between the
196 monthly mean sea-level and DAC at the nearest grid point of the DAC product.

197

198 **2.3 Coastal hydrographic stations**

199 Over the time window covered by this study, the Institute of Marine Research (IMR) in Bergen, Norway, has
200 maintained eight permanent hydrographic stations over the Norwegian continental shelf, at a short distance
201 from the coast (Fig. 1). Data are updated and available at
202 <http://www.imr.no/forskning/forskningsdata/stasjoner/index.html>.

203

204 Along the Norwegian coast, the number of hydrographic stations is approximately one third the number of tide
205 gauges. Therefore, compared to the tide gauges, the hydrographic stations provide a coarser spatial resolution
206 of the physical properties of the ocean. We find that the distance between adjacent hydrographic stations is
207 approximately 250 km on average. This distance is minimum between the twin stations Indre Utsira/Ytre Utsira
208 and Eggum/Skrova, where it does not exceed 30 km, whereas it is maximum in western Norway, between Bud
209 and Skrova, where it is approximately 670 km.

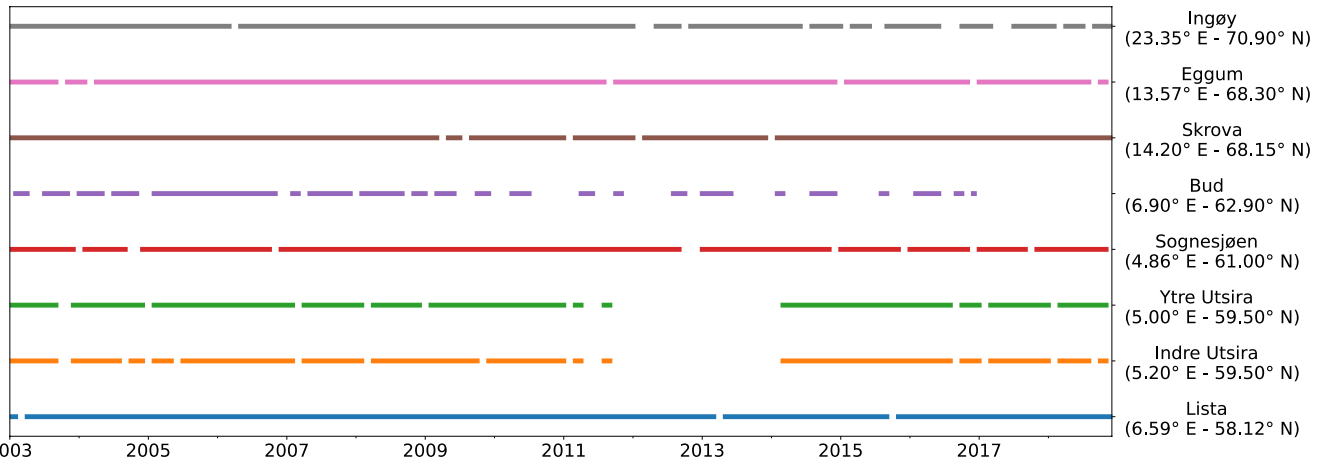
210

211 We select the temperature and salinity profiles taken between January 2003 and December 2018 for them to
212 overlap with the period covered by the ALES-reprocessed altimetry dataset. ~~The temperature and salinity~~
213 ~~profiles at each hydrographic station~~ The data are irregularly sampled, being them mostly collected once every
214 one or two weeks. To allow a comparison with the satellite altimetry dataset, we have monthly averaged the
215 temperature and salinity profiles at each hydrographic station. We should note that the monthly-averaged time
216 series of temperature and salinity ~~and~~ contain missing values (Fig. 2). Bud has the largest number of missing
217 values, with 76 gaps out of 192. It is followed by Indre Utsira and Ytre Utsira, with 44 and 41 gaps, respectively.
218 The remaining hydrographic stations have less than 16 gaps each.

219

220 The hydrographic data were used to obtain estimates of the thermosteric and the halosteric sea-level
221 components over the spatial domain considered in this study.

222



223

224

Figure 2: Data available at each hydrographic station between 01 January 2003 and 31 December 2018.

225

226 3 Methods

227 3.1 Harmonic analysis of sea-level

228 Following a similar approach to the one found in previous papers (e.g., Cipollini et al., 2017; Breili et al., 2017),
 229 we use the Levenberg-Marquardt algorithm and fit the following function to sea-level records from remote
 230 sensing and in situ data:

231

$$232 z(t) = a + b \cdot t + c \cdot \sin(2\pi t + d) + e \cdot \sin(4\pi t + f), \quad (1)$$

233

234 where a is the offset, b the linear trend, c and d the amplitude and the phase of the annual cycle, e and f the
 235 amplitude and the phase of the semi-annual cycle. Then, we compare the linear trend, the amplitude and the
 236 phase of the annual cycle, and the detrended, deseasoned sea-level signals from remote sensing and in situ
 237 data. It is important to note that the use of this formula does not account for interannual variations of the
 238 seasonal cycle.

239

240 In the present this study, we present the estimates of the sea-level trend from both satellite altimetry and the
 241 tide gauges with the corresponding 95% confidence intervals (Fig. 9). Moreover, we assess how strongly the

242 linear trends from altimetry depends on the time period considered and show those trends that are significant
 243 at a 0.05 significance level (Fig. 10). To compute the confidence intervals and the statistical significance, we
 244 account for the serial correlation in the time series. Indeed, successive values in the sea-level time series might
 245 be significantly correlated and, therefore, not drawn from a random sample. To account for this non-zero
 246 correlation, we compute the semi-variogram of the detrended and deseasoned SLA from satellite altimetry and
 247 the tide gauges and then determine the effective number of degrees of freedom, N^* , for each time series
 248 (Wackernagel, 2003), as described in Appendix A. To compute the 95% confidence interval of the linear trends,
 249 we then use formula (7) in appendix A. Together with the semi-variogram, we also estimate the effective
 250 number of degrees of freedom using the formula $N^* = N \cdot \frac{1-r_1}{1+r_1}$, where N is length of the time series and r_1 is its
 251 lag-1 autocorrelation (Bartlett, 1935). However, in this paper, we opt for the more stringent approach and only
 252 present the confidence interval derived using the semi-variograms. Indeed, we find that the semi-variogram
 253 approach returns either the same or fewer effective number of degrees of freedom (not shown) when
 254 compared to the other method. This is not the case for the effective number of the degrees of freedom of the
 255 detrended and deseasoned SLA difference between ALES and the tide gauges. However, we find that the choice
 256 of the approach does not alter our conclusions.

257

258

259 ~~We compute the 95% confidence interval of the linear trend as follows:~~

260

$$CI = t_{0.05/2, N^*-6} \cdot \frac{\sqrt{N-1}}{\sqrt{N^*-1}} \cdot SE$$

261 ~~Where SE is the standard error of the linear trend, computed as if $N^* = N$, the total number of observations in~~
 262 ~~the time series, and $t_{0.05/2, N^*-6}$ is the t value computed using $N^* - 6$ degrees of freedom at a 0.05~~
 263 ~~significance level.~~

264

265 3.2 Colocation of satellite altimetry and tide gauges

266 To compare the sea-level from satellite altimetry and tide gauges, we first need to preprocess the altimetry
 267 observations since these are not collocated neither in space nor in time with the tide gauges. The collocation

268 consists of two steps. At first, we select the altimetry observations that are located nearby each tide gauge.
269 Then, we average these observations both in space and in time to create, for each tide gauge location, a single
270 time series of monthly mean sea-level anomaly from altimetry.

271

272 ~~During the process, we verify that the selected altimetry observations represent the sea level variability at each~~
273 ~~tide gauge location. More precisely, since tide gauges represent the sea level variability along a stretch of the~~
274 ~~coast, the distance from the coast and along the coast are adjustable parameters of the selection window. At~~
275 ~~each station, we test different combinations of the two distances, with the first ranging between 5 and 20 km~~
276 ~~and the second between 20 and 200 km. Then, we pick the combination that maximizes the linear correlation~~
277 ~~coefficient between the detrended and deseasoned SLA measured by satellite altimetry and by the tide gauge~~
278 ~~(as, for example, in Cipollini et al., 2017). To select the minimum and the maximum distances from the coast, we~~
279 ~~have proceeded as follows. We have set the minimum distance from the coast following the recommendations~~
280 ~~on how to use the ALES dataset: these recommend to discard data within 3 km from the coast. We have then~~
281 ~~performed a sensitivity analysis and found only small differences between the results obtained applying a~~
282 ~~maximum distance from the coast of either 40 km or 20 km. To only focus on the observations over the~~
283 ~~continental shelf, we have selected the range of distances from the coast between 5 and 20 km. Similarly, we~~
284 ~~have performed a sensitivity test on the distance from the tide gauge allowing it to range between 15 and 400~~
285 ~~km: as before, we have found little difference in the final results.~~

286

287 ~~We choose to maximize the linear correlation coefficient, instead of minimizing the root mean square~~
288 ~~differences (RMSDs), since the former appears less sensitive in cases when there are few altimetry~~
289 ~~observations. There are three exceptions: the Stavanger, Trondheim and Bodø tide gauges, where a very~~
290 ~~stringent colocation accidentally yields a high correlation. Thus, for Bodø for these three stations, we select the~~
291 ~~second highest correlation, which corresponds to a distance from the coast of 20 km and to a distance along the~~
292 ~~coast of 200 km.~~

293

294 ~~The results suggest that the spatial pattern associated with the detrended and deseasoned sea level anomaly~~
295 ~~extends over hundreds of kilometres. Indeed, the maximum values of the linear correlation coefficients occur~~
296 ~~for distances along the coast that range between 140 and 200 km, with them being 200 km at 13 out of 22 tide~~

297 ~~gauges. Moreover, when, for each tide gauge, we manually set the distance from the coast and along the coast,~~
298 ~~respectively, to 20 km and 200 km, we find that both the linear correlation coefficient and the RMSD vary only~~
299 ~~little: the first changes by less than 5 %, whereas the second by less than 4.5 %.~~

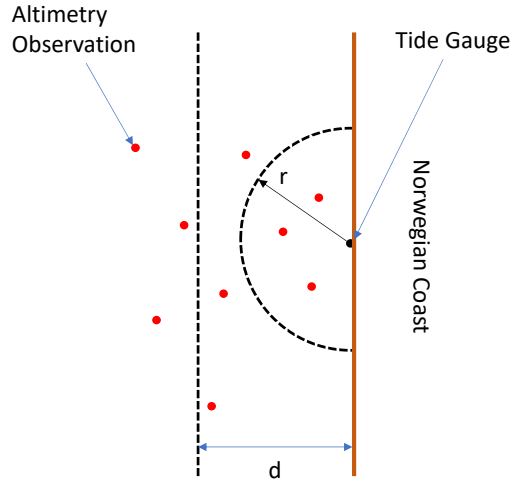
300

301 During the process, we verify that the selected altimetry observations represent the sea-level variability at each
302 tide gauge location. More precisely, since tide gauges represent the sea-level variability along a stretch of the
303 coast, we monthly average all the altimetry observations within a certain distance “d” from the coast and a
304 certain radius “r” from the tide gauge (Fig. 3). We try different combinations of d and r by allowing the first to
305 range between 5 and 20 km, with steps of 2.5 km, and the second between 20 and 200 km, with steps of 15 km.
306 Then, we pick the combination that maximizes the linear correlation coefficient between the detrended and
307 deseasoned SLA measured by satellite altimetry and by the tide gauge (as, for example, in Cipollini et al., 2017).
308 To set the maximum values of d and r at 20 and 200 km respectively, we have first performed a sensitivity test
309 and noted that larger values of d and r return slightly higher linear correlation coefficients (especially in
310 northern Norway), but do not alter the main results of this study. At the same time, a maximum distance of 20
311 km from the coast and of 200 km from the tide gauge ensures that all the selected altimetry points are located
312 over the continental shelf and that we can better capture the spatial scale variability of the seasonal cycle of the
313 sea level and of the sea-level trend.

314

315 We use the process described above to build a time series of monthly mean sea-level anomaly from altimetry at
316 each tide gauge location. The resulting sea-level time series have no missing values between Viker and Bodø.
317 Instead, to the north of Bodø, they have 29 missing values which result from the lack of altimetry observations
318 between November 2010 and March 2013.

319



320

321 **Figure 3: Sketch to illustrate the procedure used to build a monthly averaged SLA time series from the ALES-reprocessed satellite**
 322 **altimetry dataset at each tide gauge location. The parameter r is the distance from the tide gauge, whereas d is the distance from**
 323 **the coast.**

324 3.3 Colocation of satellite altimetry and hydrographic stations

325 We preprocess the altimetry observations to examine the steric contribution to the sea-level variability budget
 326 at each hydrographic station since the two datasets are not colocated neither in space nor in time. More
 327 precisely, we select all the altimetry observations located within 20 km from the Norwegian coast and within
 328 200 km from each hydrographic station. Then, for each station, we monthly average the altimetry observations
 329 to build a sea-level anomaly time series from altimetry. The results in the previous subsection give confidence
 330 that the monthly mean sea-level computed over such a large area is representative of the sea-level variability at
 331 each hydrographic station.

332

333 **3.4 Monthly mean thermosteric, halosteric and steric sea-level components**

334 To compute the thermosteric and the halosteric components of the sea-level variability at each hydrographic
335 station, we first monthly average the temperature and salinity profiles. Then, at each hydrographic station, we
336 compute the monthly mean thermosteric and the halosteric components of the sea-level as in Richter et al.
337 (2012):

338

$$339 \eta_t = \int \alpha(T^*, S^*) \cdot (T - T_0) dz, \quad (2)$$

$$340 \eta_s = - \int \beta(T^*, S^*) \cdot (S - S_0) dz, \quad (3)$$

341

342 where α and β are the coefficients of thermal expansion and haline contraction, both computed at $T^* = (T +$
343 $T_0)/2$ and $S^* = (S + S_0)/2$. For each hydrographic station, T_0 and S_0 are reference values and represent time-
344 mean temperature and salinity averaged over the entire water column (Siegismund et al., 2007).

345

346 The steric component of the sea-level at each hydrographic station, η_{st} , is simply the sum of the corresponding
347 thermosteric and halosteric components of the sea level (Gill and Niller, 1973).

348

349 **3.5 Steric contribution to the Norwegian sea level**

350 At each hydrographic station, we assess the contribution of temperature and salinity to the linear trend and the
351 seasonal cycle of the SLA, and to the detrended and deseasoned SLA.

352

353 We do not use the harmonic analysis approach to estimate the sea linear trend and the seasonal cycle of the
354 SLA and of the thermosteric, halosteric and steric components of the sea-level at each hydrographic station.
355 Instead, we use simple linear regression to estimate the linear trend and we compute the monthly climatology
356 of each detrended time series to estimate the corresponding seasonal cycle. Indeed, the seasonal cycle of the
357 SLA and of the thermosteric, halosteric and steric sea level might depart from the linear combination of the
358 annual and the semi-annual cycles. ~~We use simple linear regression to estimate the linear trend of the SLA and~~
359 ~~of the thermosteric, halosteric and steric components of the sea level. The seasonal cycle for each time series is~~

360 ~~considered a monthly climatology. We prefer this procedure over the harmonic analysis approach since the~~
361 ~~seasonal cycle of the SLA and of the thermosteric, halosteric and steric sea level might depart from the linear~~
362 ~~combination of the annual and the semi-annual cycles.~~

363

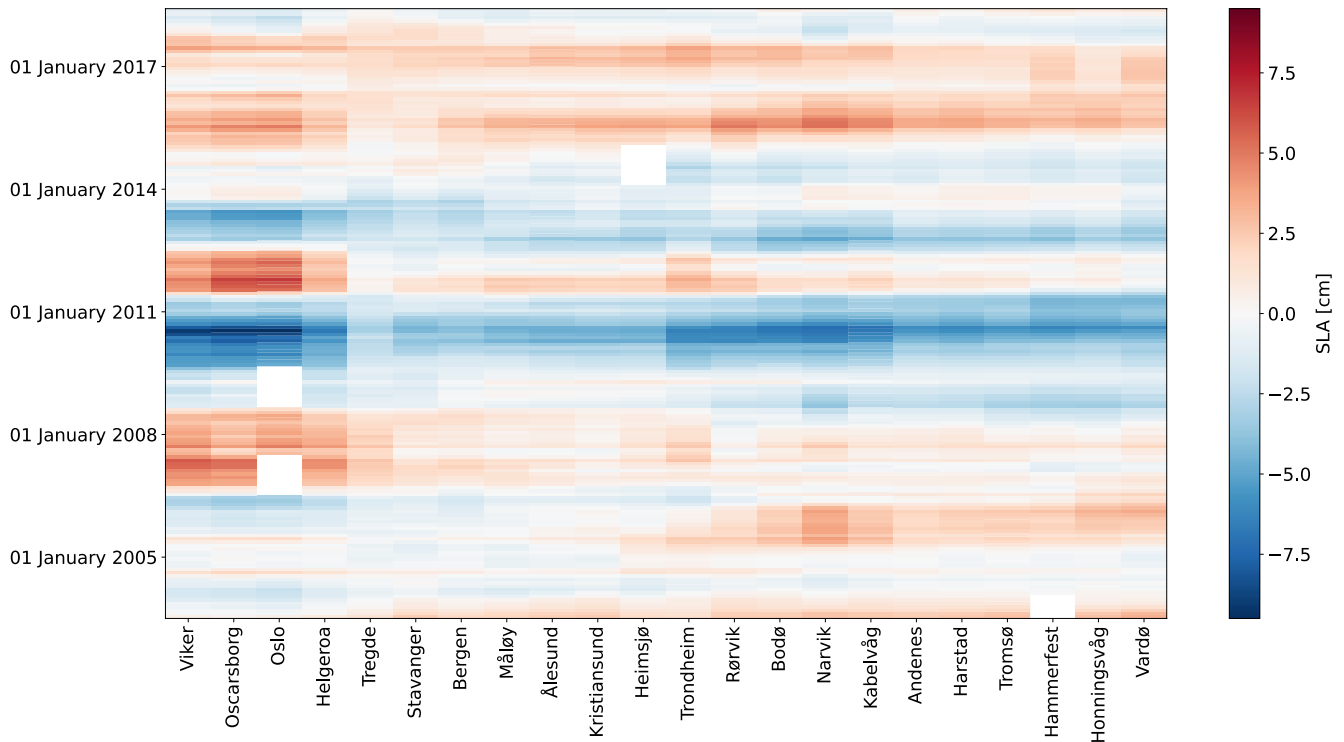
364 **4 Comparison of satellite altimetry and tide gauges measurements**

365 In this Section, we assess the quality of the ALES reprocessed coastal altimetry dataset against tide-gauge
366 records by comparing the detrended and deseasoned sea-level variability, the sea-level annual cycle and sea-
367 level trends provided by the remote-sensing and in situ data. We also focus on the stability of linear trend
368 estimates obtained from satellite altimetry (Liebmann et al., 2010; Bonaduce et al., 2016).

369

370 **4.1 Detrended and deseasoned coastal sea-level**

371

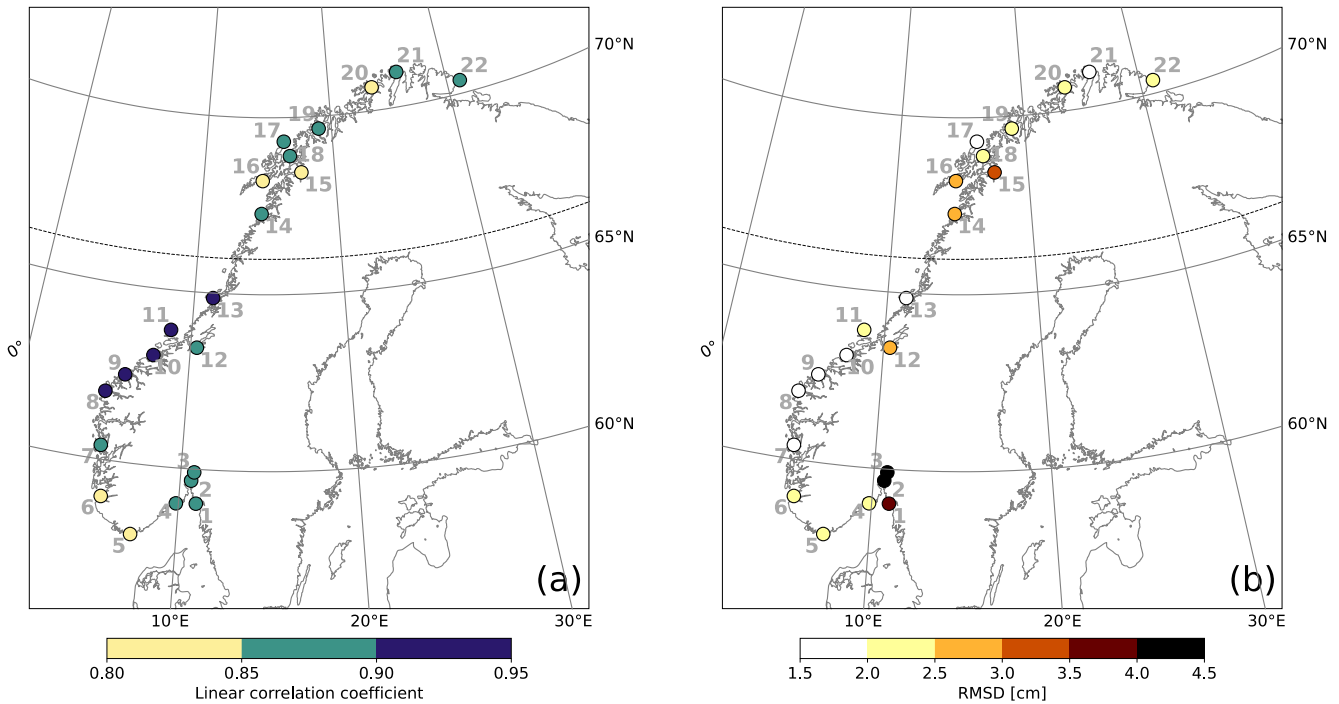


372
 373 **Figure 4: Hovmöller diagram of the detrended and deseasoned monthly mean SLA from tide gauges. The SLA at each tide gauge has**
 374 **been low-pass filtered with a one-year running mean. The tide gauges are displayed on the x-axis. Time is displayed on the y-axis and**
 375 **increases from bottom to top.**
 376

377
 378 Before comparing the detrended and deseasoned SLA from altimetry and tide gauges, we briefly describe how
 379 the detrended and deseasoned SLA evolves along the Norwegian coast during the period under study. More
 380 precisely, we low-pass filter the detrended and deseasoned SLAs with a one-year running mean to identify their
 381 main features at each tide gauge location. Figure 4 shows years when the detrended and deseasoned SLA
 382 variations are coherent along the whole Norwegian coast, and years when the sea-level variability occurs at
 383 smaller spatial scales (between 100 and 1000 km). As an example, between mid-2009 and the beginning of 2011
 384 circa, the detrended and deseasoned SLA shows negative values of up to -6 cm along the entire Norwegian
 385 coast. On the contrary, between 2003 and mid-2009, we note a dipole pattern, with SLA with opposite sign in
 386 the south and in the north of Norway. Indeed, up to the beginning of 2006 circa, the Norwegian coast has
 387 experienced a negative SLA values to the south of Hemsjø and a positive SLA to the north of Hemsjø. Over
 388 During the following three years, the opposite situation has occurred. These results suggest that, although

389 coherent sea-level variability occurs along the Norwegian coast as seen from tide gauges, there are periods
 390 when it does not: during these periods, the sea-level variability is likely driven by local changes.
 391

1 - Viker	4 - Helgeroa	7 - Bergen	10 - Kristiansund	13 - Rørvik	16 - Kabelvåg	19 - Tromsø	21 - Honningsvåg
2 - Oscarsborg	5 - Tregde	8 - Måløy	11 - Heimsjø	14 - Bodø	17 - Andenes	20 - Hammerfest	22 - Vardø
3 - Oslo	6 - Stavanger	9 - Ålesund	12 - Trondheim	15 - Narvik	18 - Harstad		

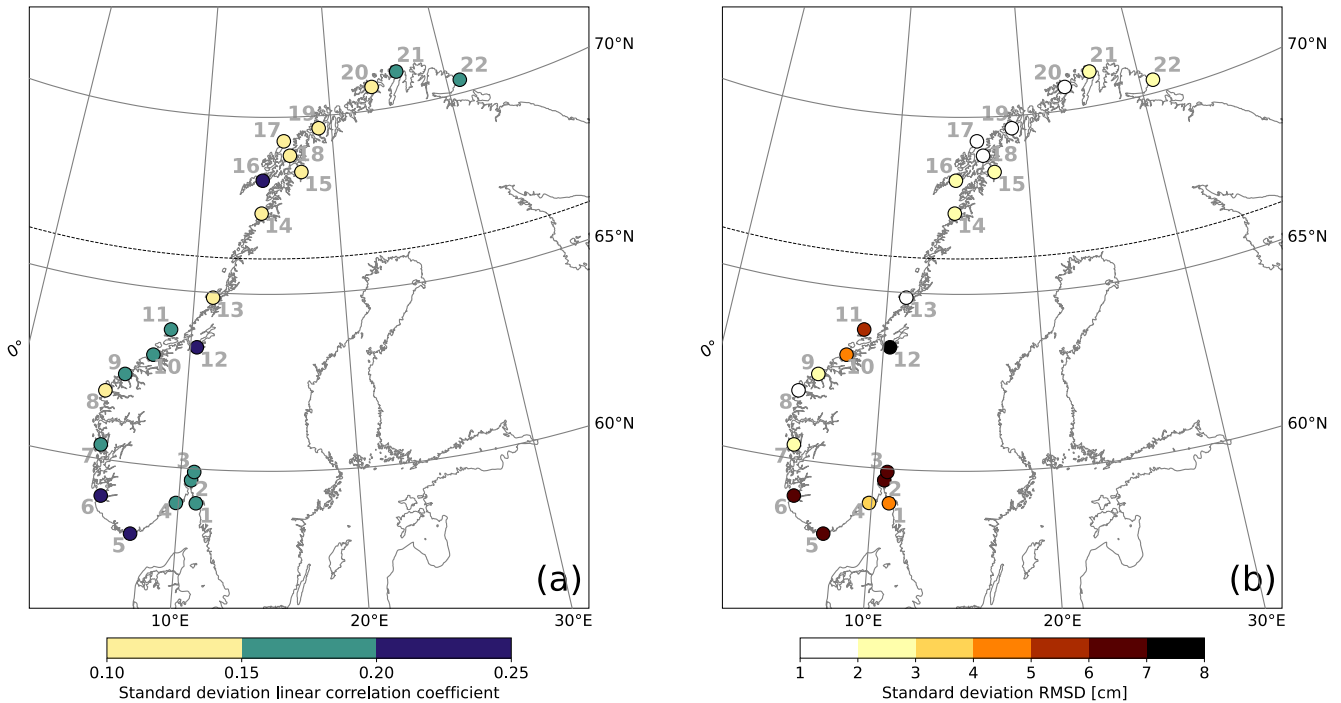


392
 393 **Figure 5: Comparison between coastal sea-level signals from in situ measurements and area-averaged remote-sensing data. At each**
 394 **tide gauge location, linear correlation coefficient (a) and RMSD (b) between the detrended and deseasoned monthly mean SLA from**
 395 **the ALES altimetry dataset and from the tide gauge. The black, dashed line indicates the 66° N parallel.**
 396

397 Figure 5 shows a very good agreement between the detrended and deseasoned monthly mean SLA from ALES
 398 and the tide gauges. The two datasets agree best along the west coast of Norway where, if we exclude
 399 Trondheim, the linear correlation coefficients exceed 0.90 and the RMSDs range between 1.5 and 2.5 cm. As
 400 expected, satellite altimetry performs better between Måløy and Rørvik than in southern and northern Norway
 401 because of the convergence of altimeter tracks in the region. We suspect that Trondheim is an exception
 402 because it is located in the Trondheim fjord, where satellite altimetry might not adequately capture local sea-
 403 level variations: the presence of land and patches of calm water affects the quality of the satellite altimetry
 404 measurements (Gómez-Enri et al., 2010; Abulaitijiang et al., 2015), and the complex bathymetry and coastline

405 hamper geophysical corrections (Cipollini et al., 2010). Similar peculiarities of the coastline along the Norwegian
 406 Trench, in the Skagerrak and in the Oslo fjord, are also likely to affect the agreement, causing the linear
 407 correlation coefficients to fall between 0.80 and 0.90 and the highest RMSDs to range between 2.5 and 4.5 cm.
 408 Instead, in northern Norway, where we find linear correlation coefficients between 0.80 and 0.90 (statistically
 409 significant at a 0.05 significance level) and RMSDs between 1.5 and 3 cm, the problem might result from the
 410 smaller number of altimetry observations in the region. Indeed, only the tracks of Envisat, SARAL, SARAL drifting
 411 phase, Sentinel 3A and 3B cover the Norwegian coast north of 66° N.
 412

1 - Viker	4 - Helgeroa	7 - Bergen	10 - Kristiansund	13 - Rørvik	16 - Kabelvåg	19 - Tromsø	21 - Honningsvåg
2 - Oscarsborg	5 - Tregde	8 - Måløy	11 - Heimsjø	14 - Bodø	17 - Andenes	20 - Hammerfest	22 - Vardø
3 - Oslo	6 - Stavanger	9 - Ålesund	12 - Trondheim	15 - Narvik	18 - Harstad		



413
 414 **Figure 6: Comparison between coastal sea-level signals from in situ measurements and area-averaged remote-sensing data. At each**
 415 **tide gauge location, standard deviation of the linear correlation coefficients (a) and of the RMSDs (b) computed over each possible**
 416 **combination of the distance from the coast and of the distance from the tide gauge. The black, dashed line indicates the 66° N**
 417 **parallel.**
 418

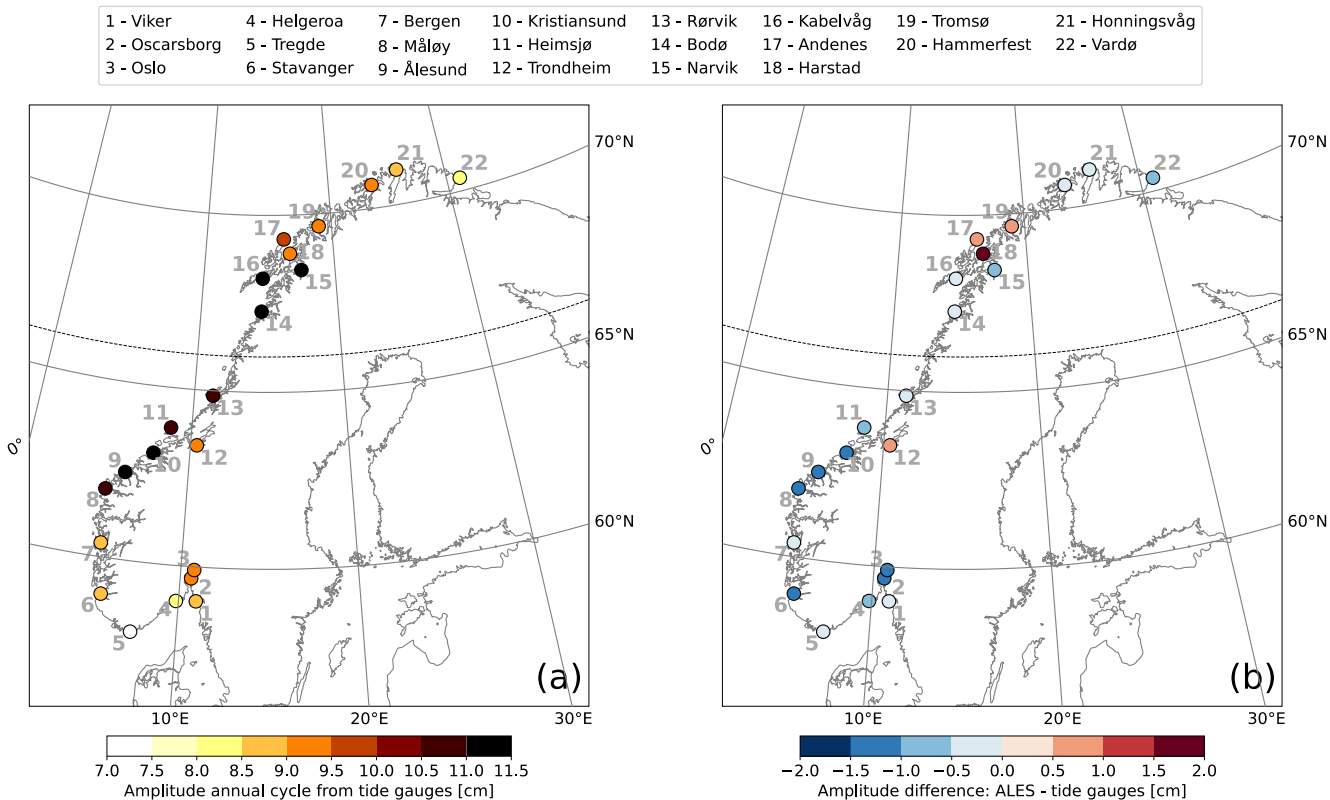
419 The complex geometry of the Norwegian coast can lead to small scale variations in sea level. This can partly
 420 explain the difference between the sea level estimates from tide gauges and from altimetry. Indeed, while the

421 SLA time series measured by the tide gauges are representative for particular locations, those from satellite
422 altimetry, preprocessed as described above, are representative for a spatial domain around the tide gauge
423 positions. Here, we give an estimate of the geometrical uncertainty on the SLA estimates from satellite
424 altimetry by computing the standard deviation of the linear correlation coefficient and of the RMSD over all the
425 possible combinations of the distance from the coast and of the distance along the coast, as shown in Fig. 6.

426
427 These results suggests that the detrended and deseasoned SLA in the south vary over smaller spatial scales
428 compared to the north. Indeed, both the linear correlation coefficient and the RMSD in southern Norway
429 depend more on the size of the selection window than in northern Norway. In Fig. 6a, we note that the
430 standard deviation of the linear correlation coefficients mainly ranges between 0.15 and 0.25 to the south of
431 Trondheim, whereas it ranges between 0.10 and 0.15 to the north of Trondheim. Likewise, the standard
432 deviation of the RMSD follows a similar spatial pattern, with southern Norway showing higher values compared
433 to northern Norway.

434
435 Figure 6 supports our previous conclusions on the relationship between satellite altimetry and the tide gauges
436 at Trondheim, Oslo and Oscarborg. In Figure 6, we show, for each tide gauge, the standard deviation of the
437 linear correlation coefficient and of the RMSDs over all the possible combinations of the distance from the coast
438 and from the tide gauge to measure the geometrical uncertainty of the SLA estimates from satellite altimetry.
439 We find that, at Trondheim, both the linear correlation coefficient and the RMSD depend more on the size of
440 the selection window when compared to other regions of the Norwegian coast. Similarly, at Oslo and
441 Oscarborg, we note an anomalously high standard deviation of the linear correlation coefficient. We expect
442 anomalously high values of the standard deviation of the linear correlation coefficients and RMSDs because
443 these three tide gauges are in sheltered areas (Trondheim in the Trondheim fjord, whereas Oslo and Oscarborg
444 and the Oslofjord) which can favour the formation of patches of calm water and negatively affect the quality of
445 the satellite altimetry observations.

446

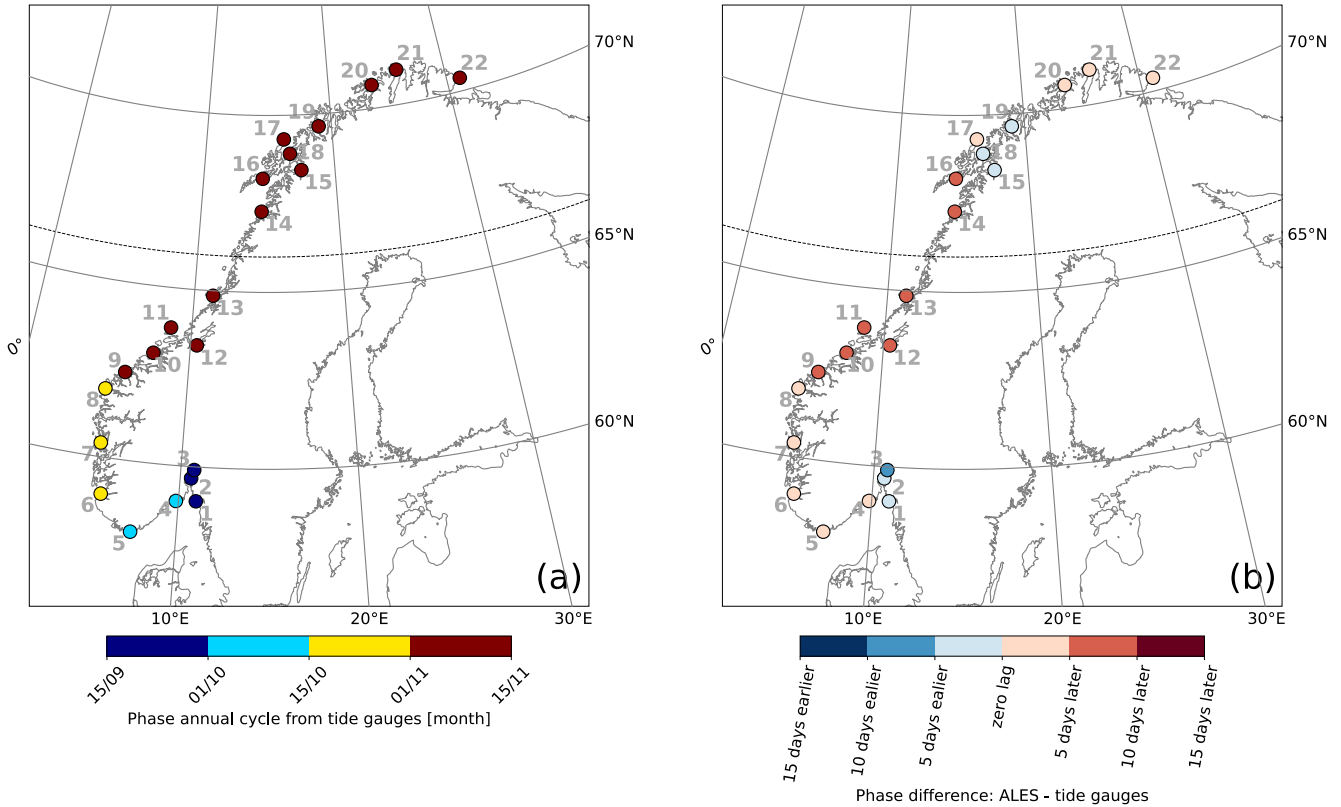


448
 449 **Figure 7: Comparison between the amplitude of coastal sea-level annual cycle from in situ measurements and area-averaged remote-**
 450 **sensing data. At each tide gauge location, amplitude of the annual cycle from the tide gauges (a) and difference between the**
 451 **amplitude of the annual cycle from the ALES-reprocessed altimetry dataset and the tide gauges (b). The black, dashed line indicates**
 452 **the 66° N parallel.**
 453

454 Figures 7 and 8 show a good agreement between the annual cycle estimated using the ALES altimetry dataset
 455 and the tide gauges. The difference between the amplitudes of the annual cycle from ALES and the tide gauges
 456 ranges between -1.2 and 1.8 cm. However, at most tide gauge locations (16 out of 22), the differences are much
 457 smaller, between -1 and 1 cm, less than 10 % of the amplitude of the corresponding annual cycle (Fig. 7a). We
 458 note that the differences between the amplitudes are mostly negative along the southern and western coast of
 459 Norway and that, to the north of Rørvik, they become smaller, and even change sign at some locations (Fig. 7b).
 460
 461 The difference between the phases of the annual cycle estimated using the ALES altimetry dataset and the tide
 462 gauges ranges between -10 and +10 days (Fig. 8b). Such a great similarity indicates that both radar altimetry

463 and the tide gauges capture the phase lag of approximately two months between the annual cycle in the north
 464 and in the south of Norway. The annual cycle peaks during the second half of September in the Skagerrak and in
 465 the Oslofjord region, in October along the Norwegian Trench and in south-west Norway, and mainly during the
 466 first week of November north of Kristiansund.
 467

1 - Viker	4 - Helgeroa	7 - Bergen	10 - Kristiansund	13 - Rørvik	16 - Kabelvåg	19 - Tromsø	21 - Honningsvåg
2 - Oscarsborg	5 - Tregde	8 - Måløy	11 - Heimsjø	14 - Bodø	17 - Andenes	20 - Hammerfest	22 - Vardø
3 - Oslo	6 - Stavanger	9 - Ålesund	12 - Trondheim	15 - Narvik	18 - Harstad		

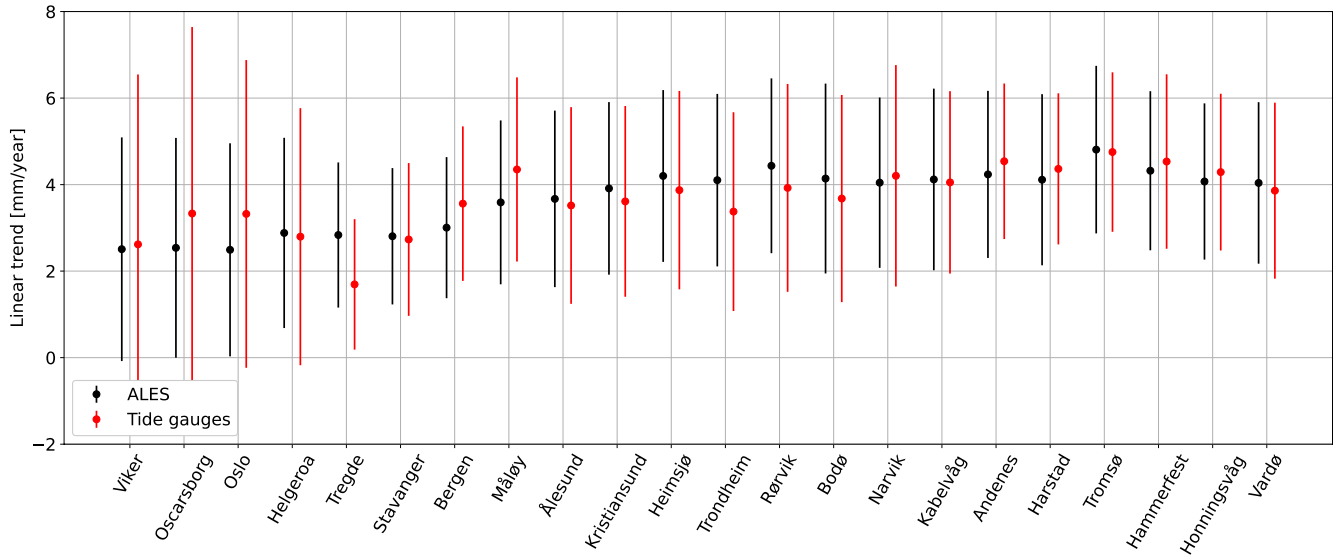


468
 469 **Figure 8: Comparison between the phase of coastal sea-level annual cycle from in situ measurements and area-averaged remote-**
 470 **sensing data. At each tide gauge location, phase of the annual cycle from the tide gauges (a) and phase difference of the annual cycle**
 471 **from the ALES-reprocessed altimetry dataset and from the tide gauges (b). The black, dashed line indicates the 66° N parallel.**

472

473

474 **4.3 Linear trend of coastal sea-level**



475
476 **Figure 9: At each tide gauge location, linear trend of the SLA from the ALES-reprocessed altimetry dataset (black dots) and from tide**
477 **gauges (red dots). The error bars show the 95th confidence intervals of the sea-level trend at each tide gauge location.**
478

479 The differences between sea-level trend estimates obtained from the in-situ and remote-sensed signals range
480 between -0.85 and 1.15 mm year⁻¹ along the Norwegian coast (Fig. 9). Both datasets return a similar spatial
481 dependence of the sea-level trend along the Norwegian coast, with the lowest values found in the Skagerrak
482 and the Oslofjord (between 2 and 3 mm year⁻¹), and the highest to the north of Heimsjø (around 4 mm year⁻¹).
483 Moreover, the two datasets return a similar uncertainty of the sea-level trend at each tide gauge location.

484
485 Despite their similarities, we still find that the difference between the sea-level trend from altimetry and tide
486 gauges is significantly different from zero at a 0.05 significance level at 3 out of 22 tide gauges. Following
487 Benveniste et al. (2020), we assess the significance in terms of fractional differences (FDs). Fractional
488 differences are defined as $FD = |\tau| / (t_{0.05/2} \cdot SE \cdot \frac{N}{N^*})$, where $|\tau|$ is the absolute value of the linear
489 trend of the SLA difference between altimetry and each tide gauge, $t_{0.05/2}$ is the critical value of the Student t-
490 test distribution for a 95 % confidence level with $N^* - 2$ number of degrees of freedom, SE is the standard
491 error, and N/N^* is the ratio between the total number of observations and the effective number of degrees of
492 freedom. When $FD > 1$, the difference between the two trends is statistically significant at a 0.05 significance

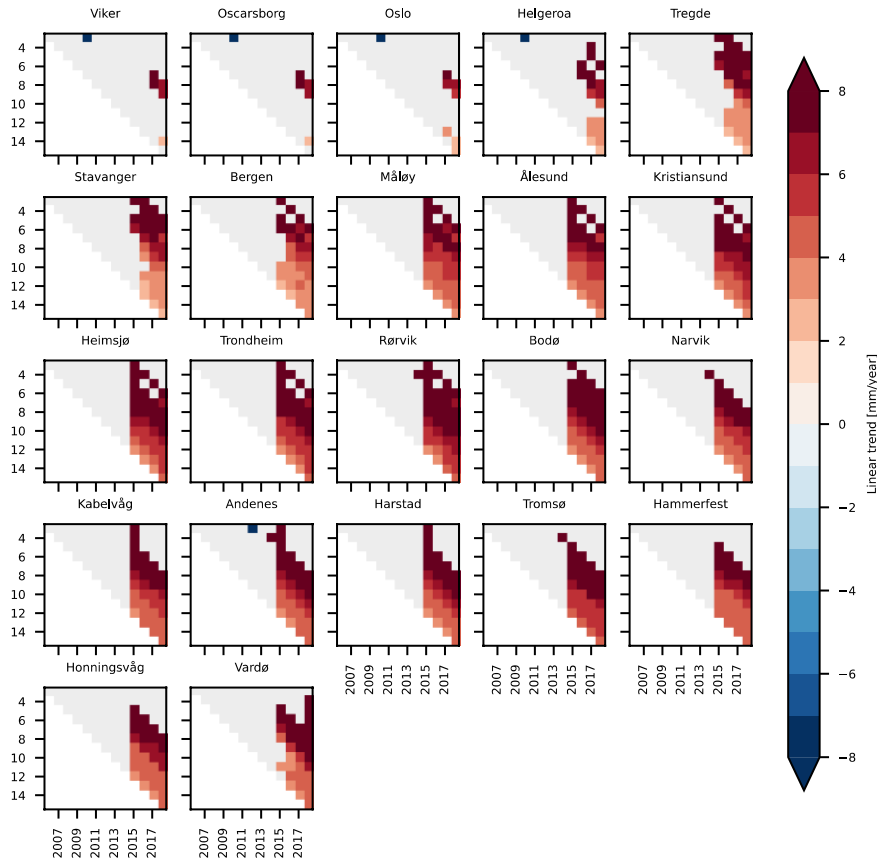
493 level, a condition that occurs at Tregde, Måløy, and Bergen. Interestingly, none of these tide gauges is located
494 north of 66° N despite only some of the altimetry missions considered in this study have an inclination
495 exceeding 66° N (namely, Envisat, SARAL, SARAL drifting phase, ~~Sentinel 3A and 3B~~). Therefore, the fewer
496 altimetry observations to the north of 66° N seem not to deteriorate the agreement between the ALES-
497 reprocessed altimetry and the tide gauges.

498

499 Following Liebmann et al. (2010), we use the satellite altimetry data to assess how strongly the sea-level trend
500 depends on the time length of the period considered. Each point in Fig. 10 shows the sea-level trend computed
501 over the number of the years on the y-axis, up to the year specified on the x-axis. Between 2003 and 2013 circa,
502 we do not find a significant sea-level trend along the Norwegian coast. Indeed, with very few exceptions, the
503 trends are not statistically different from zero at a 0.05 significance level. The exceptions consist in a small
504 number of cases, each characterized by a sea-level trend lower than -4 mm year^{-1} .

505

506 On the contrary, with the exception of three southernmost tide gauge locations, we note a significant positive
507 sea-level trend along the entire coast of Norway when the period considered for the calculation ends in 2015 or
508 later. The linear trends decrease as the length of the period selected increases. When sea-level rates are
509 computed over periods of a few years only, they even exceed 6 mm year^{-1} . Instead, over longer periods of time
510 (e.g., more than 10 years), they mainly range between 3 and 5 mm year^{-1} . A visual inspection of the time series
511 confirms that the sea-level has increased since 2014.



512
 513 **Figure 10: Stability of the sea-level trend along the Norwegian coast. At each tide gauge location, linear trend of the SLA from ALES as**
 514 **a function of the period considered. Each subplot refers to a tide gauge location and shows all the possible trends computed up to the**
 515 **year shown in the x-axis, considering the number of years displayed on the y-axis. For example, the point (x=2014, y=5) in each**
 516 **subplot shows the linear trend of the SLA computed over the 5 years period between 01 January 2009 and 31 December 2014. The**
 517 **light gray colour is used to mask those values that are not significantly different from zero at 0.05 significance level.**
 518

519

520 5 Steric contribution to the sea-level variability

521 In this Section, we use the Norwegian set of hydrographic stations to assess how temperature and salinity affect
 522 the sea-level trend, the seasonal cycle of sea-level and the detrended, deseasoned sea-level variability at
 523 different locations along the Norwegian coast.

524

525 **5.1 Variability of the thermosteric and the halosteric sea-level components**

526 The variability of the thermosteric and the halosteric sea-level components along the Norwegian coast mainly
527 occurs over two different spatial and temporal scales (Fig. 11). Notably, the seasonal cycle dominates the
528 thermosteric sea-level variability at each hydrographic station and is responsible for the thermosteric sea-level
529 to vary approximately uniformly along the coast of Norway. On the contrary, the halosteric component shows a
530 variability at shorter spatial- and temporal-scales, possibly due to the contributions from local rivers. The main
531 exceptions are, due to their proximity, the two sets of twin hydrographic stations, Indre Utsira-Ytre Utsira and
532 Eggum-Skrova (Fig. 1).

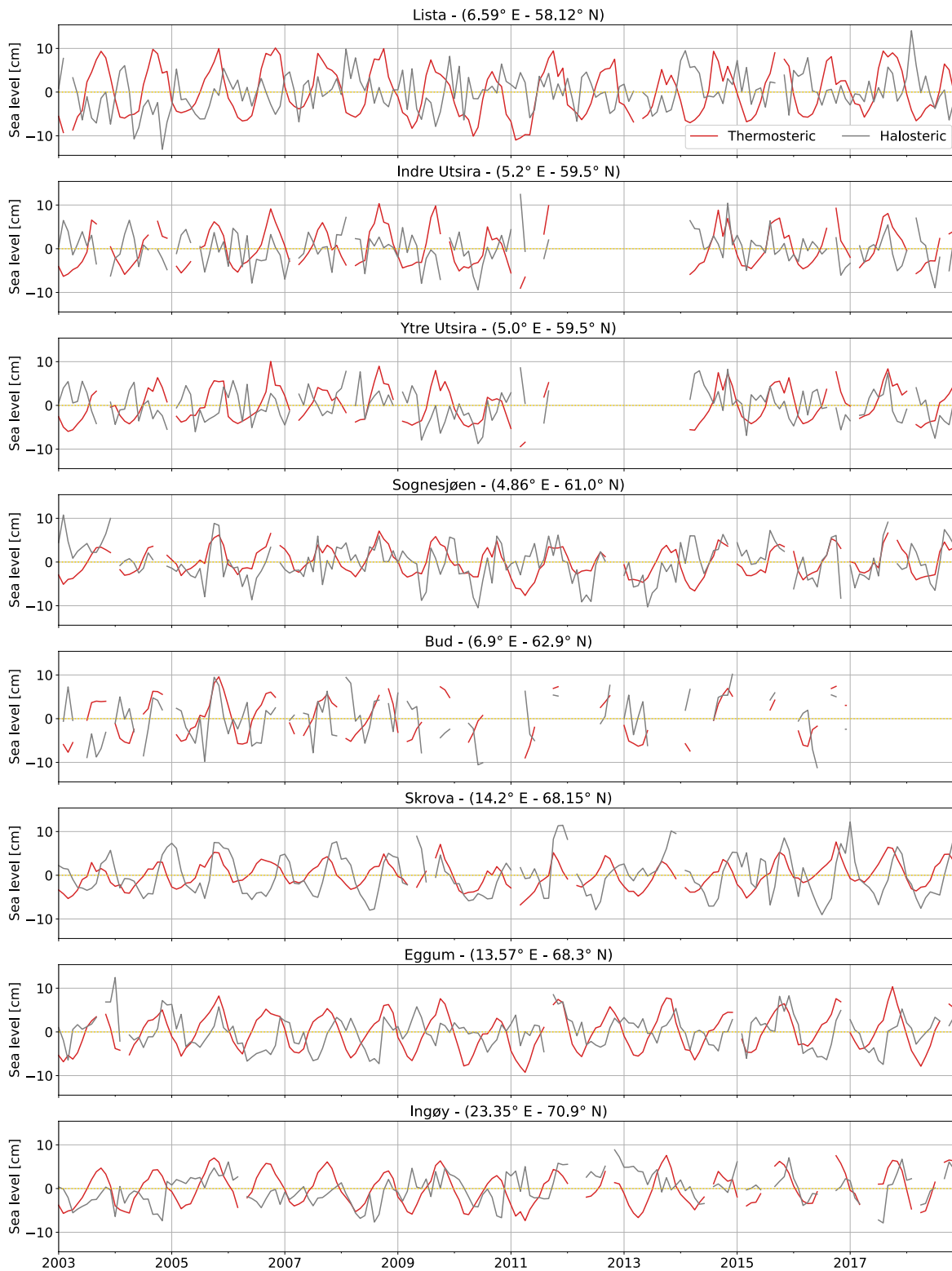
533

534 Despite these differences, both the thermosteric and the halosteric components of the sea level give a
535 comparable contribution to the sea-level variability along the Norwegian coast (Fig. 11). This ranges
536 approximately between -10 and 10 cm at each hydrographic station.

537

538 In the following sections, we investigate the spatial variability of these two components along the Norwegian
539 coast, focusing on the linear trend, the seasonal cycle, and the residuals, and on their contribution to the sea-
540 level variability in the region.

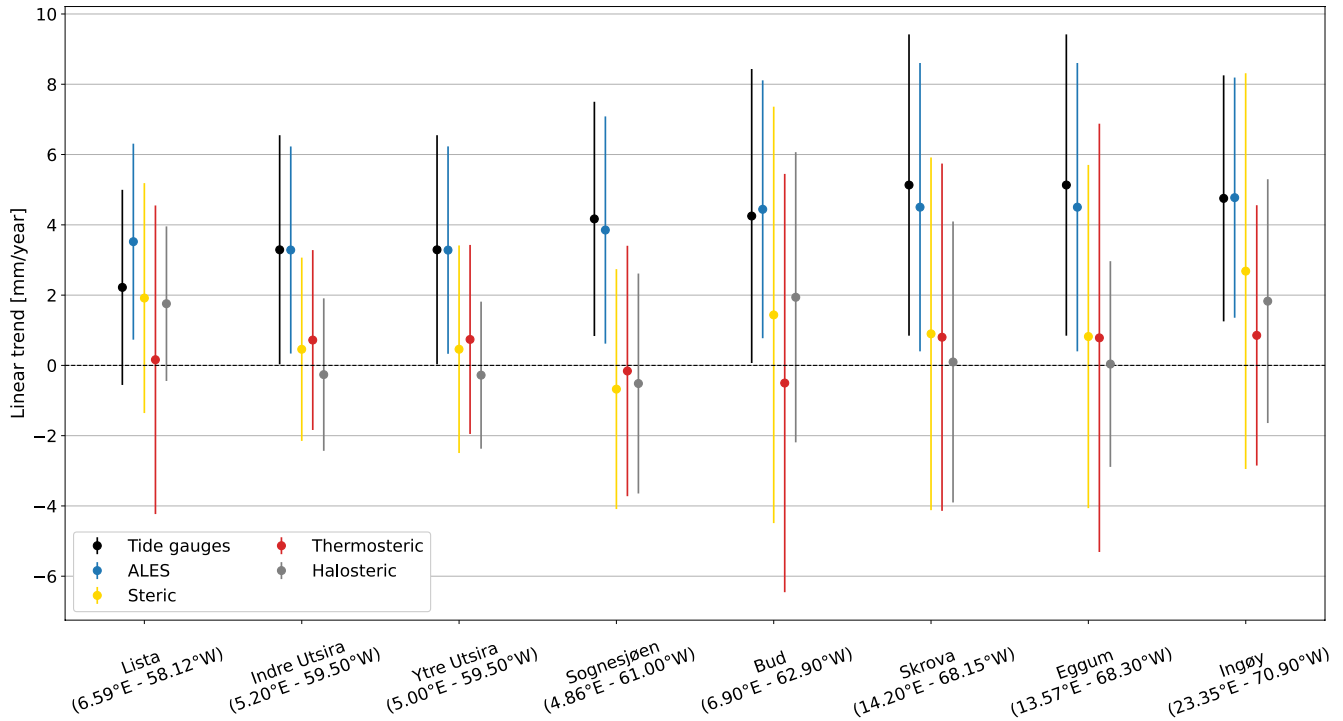
541



543 **Figure 11: Thermosteric (red) and halosteric (gray) components of the sea-level anomaly at each hydrographic station along the**
 544 **Norwegian coast.**
 545

546 **5.2 Steric contribution to the sea-level trend**

547



548 **Figure 12: At each hydrographic station, linear trend of the sea-level from tide gauges and from ALES (black and blue dots**
 549 **respectively), and of the steric, thermosteric and halosteric components of the sea level (yellow, red and gray dots respectively). The**
 550 **bars indicate the 95 % confidence intervals.**
 551
 552

553 In this section, we perform a fit-for-purpose assessment of the Norwegian hydrographic station network to
 554 obtain estimates of the steric sea-level trends from satellite altimetry and in-situ data.

555

556 Over the period 2003-2018, we find that the linear trends of the thermosteric, halosteric and steric components
 557 of the sea level approximately range between -1.0 and 2.5 mm year⁻¹. The steric contributions to coastal sea-
 558 level trends experience a large spatial variability, with it being even negative at Sognesjøen and reaching a peak
 559 of approximately 55% of the sea-level trend estimated from satellite altimetry at Lista and Ingøy. Moreover,

560 when we compare the thermosteric and the halosteric signals at these locations, we note that the latter
561 contributes more than the former to the coastal sea-level trends (up to 55% of the sea-level trend from
562 altimetry). The width of their confidence intervals of the thermosteric, halosteric and steric contributions
563 ranges between 4.0 and 12.0 mm year⁻¹ circa, with northern Norway exhibiting larger uncertainties (Fig. 12).
564 This is a result of the high inter-annual variability of the thermosteric and the halosteric components in the
565 region (Figs. B1 and B4), which leads to a fewer effective number of effective degrees of freedom and,
566 therefore, to less accurate estimates of the linear trend.

567

568 We also test if using tide gauges, instead of satellite altimetry, could alter our estimates of the relative
569 contribution of these components (thermosteric, halosteric and steric) to the sea-level trend along the coast of
570 Norway. Such alteration may indeed occur because the sea-level variations measured by the Norwegian tide
571 gauges might not properly represent those occurring in proximity of the hydrographic stations since the two
572 sets of instruments are not colocated in space (Fig. 1).

573

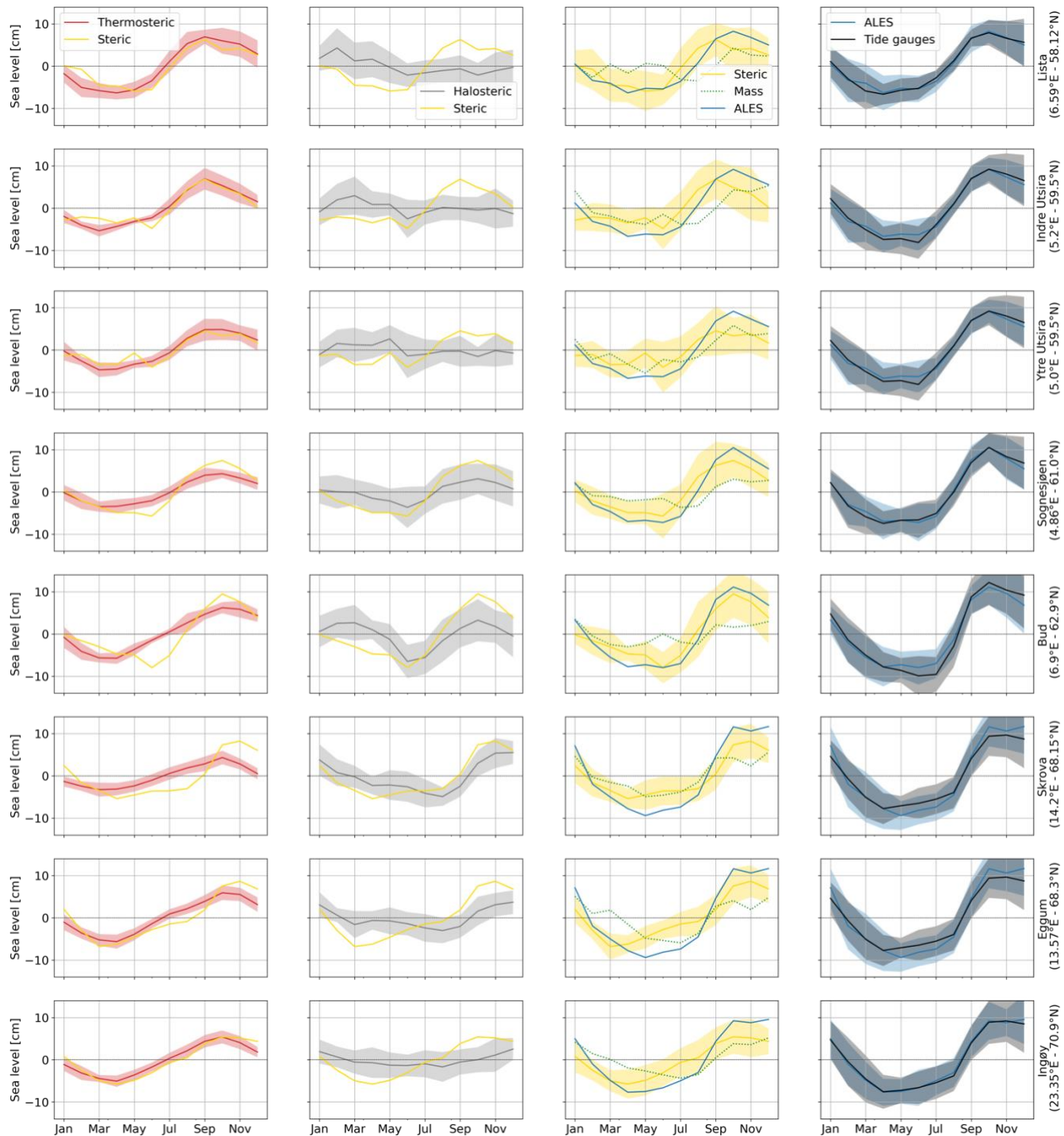
574 With the exception of Lista, the choice of the dataset has minimal influence on the estimates of the
575 thermosteric, halosteric and steric relative contributions to the sea-level trend along the coast of Norway. We
576 reach this conclusion by visual inspection, but we also provide a more quantitative analysis based on the ratio
577 between the linear-trend of the SLA and of the thermosteric, halosteric and steric components of the sea-level.
578 We find that, apart from Lista, the choice of the dataset modifies such a ratio by less than 13%. At Lista, the
579 change amounts to 59% and results from the ALES-retracked satellite altimetry dataset returning a sea-level
580 trend approximately 1.6 times larger than that provided by the tide gauge at Tregde (this is the tide gauge we
581 use to compute the thermohaline contribution at Lista). Such a large variation is expected since, as we have
582 already noticed, the sea-level rates obtained considering tide gauge and satellite data at Tregde show a less
583 accurate agreement (Figs. 9 and C5).

584

585

586 **5.3 Steric contribution to the seasonal cycle of sea level**

587



588
589
590

Figure 13: Monthly climatology of the sea-level signals at the hydrographic station positions. The panels show the steric (yellow lines), thermosteric (red lines), halosteric (gray lines), and mass (green lines) components of the sea-level. The monthly climatology obtained

591 from altimetry (blue lines) and tide-gauge (black lines) measurements are also shown. The shading enveloping the monthly
 592 climatologies shows the region departing from each line by one climatological standard deviation.

593

594

595 Table 1: Comparison between the seasonal cycle of SLA from ALES, of SLA from the tide gauges and of steric sea level at each
 596 hydrographic station position. The first and the second columns show, for ALES and the tide gauges, the RMSD between the seasonal
 597 cycle of SLA and of the steric sea-level, scaled by the range (maximum minus minimum) of the seasonal cycle of SLA. The third and the
 598 fourth columns show the ratio of the amplitudes and the lag of maximum correlation of the seasonal cycle of SLA from ALES and of
 599 steric sea level.

	Scaled $RMSD_{ALES}$	Scaled $RMSD_{Tide\ gauges}$	$\frac{Amplitude_{ALES}}{Amplitude_{Steric}}$	Lag maximum correlation ALES and steric (months)
Lista (6.59°E – 58.12°N)	16%	15%	0.8	1
Indre Utsira (5.20°E – 59.50°N)	21%	23%	0.7	1
Ytre Utsira (5.00°E – 59.50°N)	21%	22%	0.6	1
Sognesjøen (4.86°E – 61.00°N)	13%	14%	0.8	0
Bud (6.90°E – 62.90°N)	12%	16%	0.9	0
Skrova (14.20°E – 68.15°N)	18%	16%	0.7	0
Eggum (13.57°E – 68.30°N)	19%	14%	0.7	0
Ingøy (23.35°E – 70.90°N)	19%	19%	0.7	0

600

601

602

603 In this section, we build on the results by Richter et al. (2012), and assess the thermosteric, halosteric and steric
604 contributions to the seasonal cycle of the sea level at each hydrographic station along the Norwegian coast.

605

606 We find that using the tide gauge data, instead of satellite altimetry measurements, only little affects the
607 estimate of the thermosteric, halosteric and steric contributions to the seasonal cycle of SLA (Fig. 13), even
608 though the tide gauges are not colocated in space with the hydrographic stations. Indeed, the seasonal cycle
609 returned by satellite altimetry at each hydrographic station strongly resembles that returned by the nearby tide
610 gauge (Fig. 13, fourth column). At the same time, the RMSD between the seasonal cycle of the SLA and steric
611 sea level, scaled by the range (maximum minus minimum) of the seasonal cycle of SLA, little depends on the
612 dataset used (Table 1, first and second columns).

613

614 We also note that density changes contribute substantially to the seasonal cycle of SLA along the Norwegian
615 coast, as shown by Fig. 13 and Table 1. The seasonal cycle of SLA and steric sea-level are 1-month out-of-phase
616 along the southern and western coast of Norway up to Yndre-Utsira, and in-phase over the remaining part of
617 the Norwegian coast. Moreover, the ratio between the range of seasonal cycles of steric sea level and of SLA
618 varies between 0.6, at Ytre Utsira, and 0.9, at Bud (Table 1, third column).

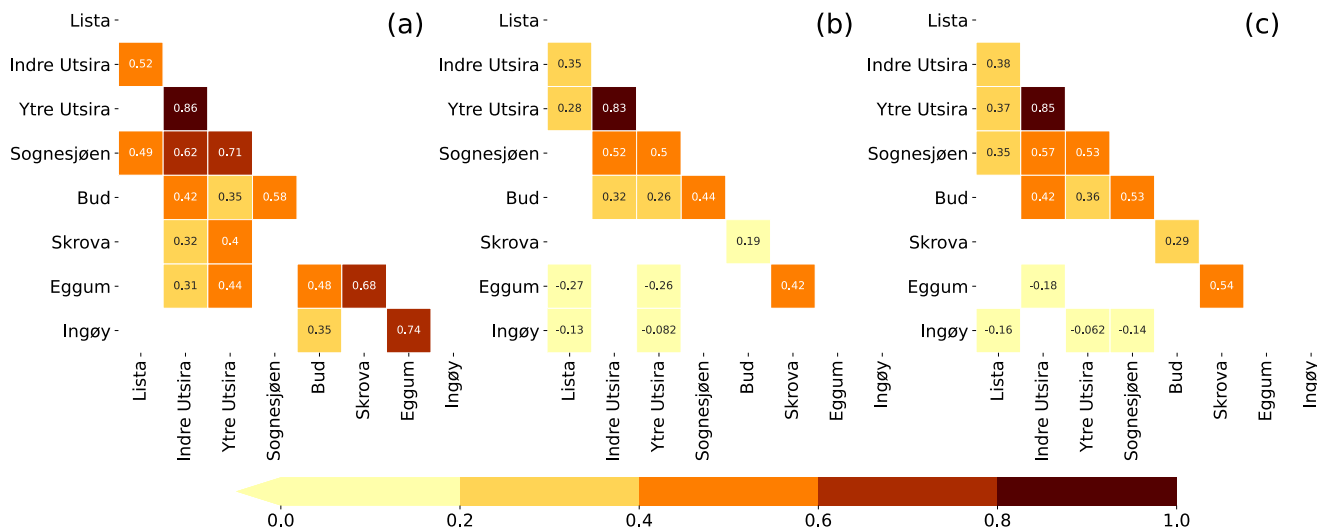
619

620 Along the Norwegian coast, the seasonal cycle of steric sea level is more affected by variations in temperature
621 than in salinity. We note that, with the exception of Bud and Skrova, the seasonal cycle of the steric component
622 mostly resembles that of the thermosteric component in terms of both amplitude and phase. At the same time,
623 we note a clear discrepancy between the seasonal cycle of the halosteric and steric components both in
624 southern Norway, where they are in anti-phase, and at Bud, where the seasonal cycle of the halosteric sea level
625 is dominated by the semi-annual cycle. A more quantitative analysis returns comparable results; the RMSD
626 between the steric and halosteric seasonal cycles exceeds by a factor of 1.4 the RMSD between the steric and
627 thermosteric seasonal cycles along the entire coast of Norway (with the exception of Skrova, where the ratio
628 between the two RMSDs is 0.7).

629

630

631 **5.4 Detrended and deseasoned coastal sea level and its components**



632
633 **Figure 14: Correlation matrices of the detrended and deseasoned thermosteric (a), halosteric (b) and steric (c) components of the sea level at each hydrographic station. Correlation values that are not significant at a 0.05 significance level have been omitted.**

634

635
636 The detrended and deseasoned thermosteric sea level along the Norwegian coast shows a larger spatial
637 variability compared to the detrended and deseasoned halosteric component (Fig. 14). The correlation matrix of
638 the thermosteric sea level (Fig. 14a) shows larger values compared to the one obtained considering the
639 halosteric sea-level signals (Fig. 14b). As an example, while the minimum linear correlation coefficient between
640 two adjacent hydrographic stations in Fig. 14a is 0.52, it is only 0.19 in Fig. 14b. We briefly discuss the small
641 spatial scale variability of the halosteric sea-level along the Norwegian coast in the Discussion and conclusions
642 section of the paper.

643

644 From Fig. 14c, we also note that the values of the correlation matrix of the steric sea-level fall in between those
645 of the thermosteric and of the halosteric components. This suggests that the thermosteric and halosteric
646 components of the sea-level give a similar contribution to the sea-level variability along the Norwegian coast.

647

648 **6 Discussion and conclusions**

649 In this paper, we have first assessed the ability of the ALES-reprocessed satellite altimetry dataset to capture
650 the Norwegian sea-level variability over a range of timescales. Then, we have used data from hydrographic
651 stations to quantify the steric contributions to the sea-level variability along the coast of Norway.

652

653 Along the Norwegian coast, the sea-level trend from the ALES-reprocessed satellite altimetry dataset is found to
654 be compatible with the estimates from tide gauges. Their difference only ranges between -0.85 and 1.15 mm
655 year⁻¹ and is significantly different from zero at the 95% confidence level at 19 out of 22 tide gauge locations.
656 Because of this good agreement, the choice of the sea-level dataset (either tide gauges or ALES) has minimal
657 impact on the estimates of the thermosteric, of the halosteric and of the steric relative contributions to the sea-
658 level trend. Despite the large uncertainties, this result is encouraging since it suggests that the ALES dataset can
659 be used to partition the sea-level variability in regions of the coastal ocean not covered by tide gauges. At the
660 same time, it confirms the validity of previous sea-level studies in the region which only used tide gauge data
661 (e.g., Richter et al., 2012).

662

663 Regarding the comparison between the ALES-retracked and the along-track (L3) conventional altimetry
664 datasets, we find that the former shows, on average, a ~~10%~~ 6% improvement, despite it being well within the
665 margins of error. This improvement is most evident at Bodø, Kabelvåg and Tromsø, in northern Norway, where
666 the agreement with the tide gauges improves by 19%, 23% and 24% respectively. The use of the ALES
667 retracker to more satellite altimetry missions, in order to have more observations and to cover the period
668 before July 2002, might help to reduce the uncertainties and return a more statistically significant result.

669

670 A comparison with Breili et al. (2017), where an along-track (L3), multi-mission conventional altimetry dataset
671 was used to analyse the sea-level trend along the Norwegian coast, returns comparable results. We cannot,
672 however, directly compare the linear trends in this work with those in Breili et al. (2017) since they focus on a
673 different period (1993-2016), and the sea-level trend along the Norwegian coast strongly depends on the length
674 of the time-window considered (Fig. 10). However, when assessing how the conventional satellite altimetry
675 datasets compare with tide-gauge records in terms of linear trend computed over a common time-window,

676 ALES shows again an improvement in northern Norway, between Bodø and Tromsø, where the difference
677 between the linear trend from ALES and the tide gauges are small (up to 0.5 mm year^{-1}), compared to circa 1 to
678 3 mm year^{-1} found by Breili et al. (2017) using a conventional altimetry dataset.

679

680 The ALES-retracked satellite altimetry dataset is found to underestimate the amplitude of the annual cycle
681 along large portions of the Norwegian coast (Fig. 7). Even though the difference between the two sets of
682 estimates is not significant at a 95% significance level (the 95% confidence interval is approximately twice the
683 standard error), we find this result interesting because of its consistency. We do not expect such a consistency
684 to depend on the ALES retracker since we find a comparable result when we use the along-track (L3)
685 conventional altimetry product (Fig. C3). We rather suspect a dependence of the amplitude of the annual cycle
686 on the bathymetry and, therefore, on the distance from the coast, as shown by Passaro et al. (2015) along the
687 Norwegian sector of the Skagerrak.

688

689 A comparison with Volkov and Pujol (2012) shows that ~~the~~ the ALES-retracked satellite altimetry better captures
690 the sea-level annual cycle along the coast of Norway with respect to the gridded sea-level altimetry products. In
691 that study, the authors have considered six tide gauges along the Norwegian coast, namely, Kristiansund,
692 Rørvik, Andenes, Hammerfest, Honningsvåg and Vardø to assess the quality of satellite altimetry maps at the
693 northern high latitudes. Except for Andenes, we note that the ALES-reprocessed coastal altimetry dataset allows
694 for more accurate estimates of the sea-level annual cycle, reducing the differences with the in situ sea-level
695 records by a factor of 3 to 6 compared to gridded satellite altimetry products.

696

697 We also assess the steric contribution to the seasonal cycle of SLA. Our results show that the steric variations
698 and, in particular, the thermosteric variations contribute considerably to the seasonal cycle of the sea level
699 along the entire Norwegian coast. Moreover, we find that the relative contributions of the thermosteric,
700 halosteric and steric sea level little depends on whether we use tide gauges or satellite altimetry. This is
701 indicative of the large-scale spatial pattern associated with the seasonal cycle of SLA.

702

703 The detrended and deseasoned sea-level variability along the Norwegian shelf resembles the along-slope wind
704 index proposed by Chafik et al. (2019). We note that the similarities between the two are stronger along the

705 western and the northern coast of Norway than in the south. Indeed, from Oslo to Ålesund, those SLA signals
706 depart from the along-slope winds index between 2003 and 2008, probably due to local effects, such as the
707 Baltic outflow. We refer to local effects since Chafik et al. (2019) attributed the interannual sea-level variability
708 over the northern European continental shelf to the along-slope winds, which might regulate the exchange of
709 water between the open ocean and the shelf through Ekman transport.

710

711 Because the detrended and deseasoned SLA pattern is coherent over large distances along the Norwegian coast
712 (see also Chafik et al., 2017), coastal altimetry observations located a few hundred kilometres apart can be
713 representative of the sea-level variations occurring at a particular tide gauge location. This explains why we can
714 average the SLA from altimetry over an area a few ~~thousands~~ hundreds of kilometres wide around each tide
715 gauge location to maximize the linear correlation coefficient between the detrended and deseasoned SLA from
716 satellite altimetry and the tide gauges (Section 3.2). Moreover, it also partly explains the good agreement
717 between satellite altimetry and tide gauges since, as we average over a large number of satellite altimetry
718 observations, we increase the temporal sampling provided by altimetry and, therefore, we reduce the noise in
719 the resulting SLA (Oelsmann et al., 2021) ~~from altimetry which might result, for example, from the rough~~
720 ~~topography of Norway.~~

721

722 The small-scale variability of the detrended and deseasoned sea-level halosteric component (Fig. 14) does not
723 reconcile with the good agreement between tide gauge sea-level signals and the ALES-reprocessed altimetry
724 dataset. Indeed, to compare the two datasets, we have averaged the satellite altimetry observations over an
725 area a few hundreds of kilometres wide around each tide gauge. However, Figure 14 suggests that the
726 estimates of the halosteric component can change significantly over an area of this size. Furthermore, while this
727 component has a magnitude comparable to that of the detrended, deseasoned SLA (not shown), it only explains
728 a small fraction (from 3 to 11 %) of the difference between the sea-level signals from altimetry and the tide
729 gauges.

730

731 Future work is thus warranted to understand whether the small-scale variability of the halosteric component of
732 the sea-level along the Norwegian coast results from measurement issues. For example, ocean salinity is
733 measured approximately once a week at Skrova and approximately twice a month at the remaining

734 hydrographic stations: this aliases the sub-weekly salinity variations into the lower frequency components and,
735 consequently, might significantly alter the monthly mean salinity values. A new study, which takes benefit from
736 ships of opportunity, synergies between different observational platforms and ocean models, could help clarify
737 this issue.

738

739 To conclude, we have demonstrated the advantage of the ALES-retracker over the conventional open ocean
740 retracker along the coast of Norway. The retracking of earlier altimeter missions would, however, be necessary
741 to provide a more accurate estimate of the sea-level variability along the coast of Norway and possibly used to
742 understand whether the sea-level in the region is accelerating. Still, this paper gives confidence that the ALES-
743 reprocessed altimetry dataset can be fruitfully used to measure coastal sea-level variations in regions poorly
744 covered by tide gauges.

745

746

747 **Appendix A**

748 To estimate the uncertainty associated with the sea-level trends derived from tide gauges and the ALES-
749 retracked satellite altimetry dataset (Fig. 9), we need to account for the effective degrees of freedom in the sea-
750 level anomaly time series. Indeed, successive points in the SLA time series might be correlated and, therefore,
751 not drawn from a random sample.

752

753 To determine the effective number of degrees of freedom, we produce the semi-variograms of the detrended
754 and deseasoned SLA from the tide gauges and the altimetry dataset. The semi-variogram is defined as:

755

$$756 \gamma(\tau) = \frac{1}{2} \cdot \text{var}[x(t) - x(t + \tau)] \quad (4)$$

757

758 where $x(t)$ is the time series under study, var stands for variance, and τ is the time lag.

759

760 The number of degrees of freedom is obtained by fitting the semi-variograms with a spherical function of the
761 form:

762

$$763 \begin{cases} c(h) = b + C_0 \cdot \left(1 - \frac{3|h|}{2a} + \frac{1|h|^3}{2a^3}\right) & \text{if } h \leq a \\ c(h) = b + C_0 & \text{if } h > a \end{cases} \quad (5)$$

764

765 where h is the fitting parameter, and a is the effective range or, in other words, the lag needed for the semi-
766 variogram to reach a constant value. Semi-variograms are preferred to autocorrelations in geostatistics because
767 they better detect the non-stationarity of time series.

768

769 We use the fit to determine the lag at which each semi-variogram reaches a plateau, since it indicates the
770 decorrelation timescale of the time series. The effective number of degrees of freedom corresponds to the ratio
771 between the length of the time series and the lag.

772

773 We find that the lag only little depends on the tide gauge location, and on whether we consider the detrended
774 and deseasoned SLA from the altimetry dataset or the tide gauges (Figs. A1 and A2). The semi-variograms
775 obtained from both altimetry and the tide gauges return a lag of 2 months at each tide gauge location, with the
776 exception of three stations in southern Norway (Viker, Oscarborg and Helgeroa), where the SLA from the tide
777 gauges is characterized by a 3-month lag.

778

779 We use the same approach to compute the uncertainty associated with the linear trend of the difference
780 between the SLA from satellite altimetry and the tide gauges, with only one exception. We noticed that the
781 spheric model does not fit the semi-variogram for Trondheim. Therefore, for Trondheim, we opted for an
782 exponential model:

783

$$784 \gamma(t) = b + C_0 \left(1 - e^{-\frac{h}{a}}\right)$$

785 (6)

786

787 where h the fitting parameter, and a is the range parameter. An exponential function is preferred over the
788 spherical function when the time series shows a strong temporal correlation.

789

790 The serial correlation is negligible along the entire Norwegian coast with the exception of Viker, Oscarborg, Oslo
791 and Narvik, where the semi-variograms return a 2-month lag (Fig. A3). At Trondheim, instead, we find a much
792 larger lag (approximately 10 months).

793

794 We use the effective number of degrees of freedom when we compute the confidence intervals of the sea-level
795 rates in Fig. 9. We compute the 95% confidence interval of the linear trend as follows:

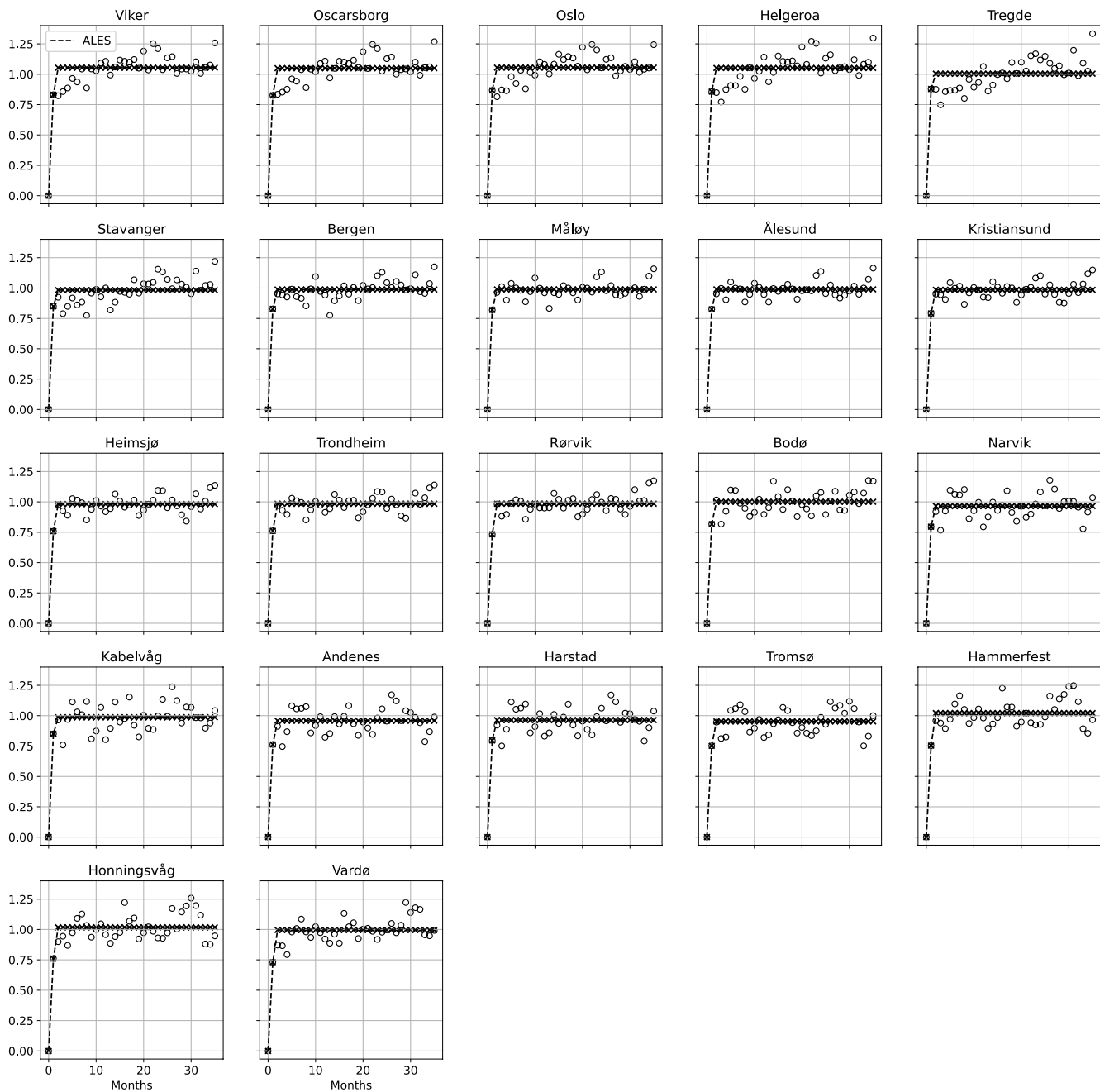
796

$$797 \quad CI = t_{0.05/2, N^*-6} \cdot \sqrt{\frac{N-1}{N^*-1}} \cdot SE \quad (7)$$

798

799 where SE is the standard error of the linear trend, computed as if $N^* = N$, the total number of observations in
800 the time series, and $t_{0.05/2, N^*-6}$ is the t-values computed using $N^* - 6$ degrees of freedom at a 0.05
801 significance level.

802



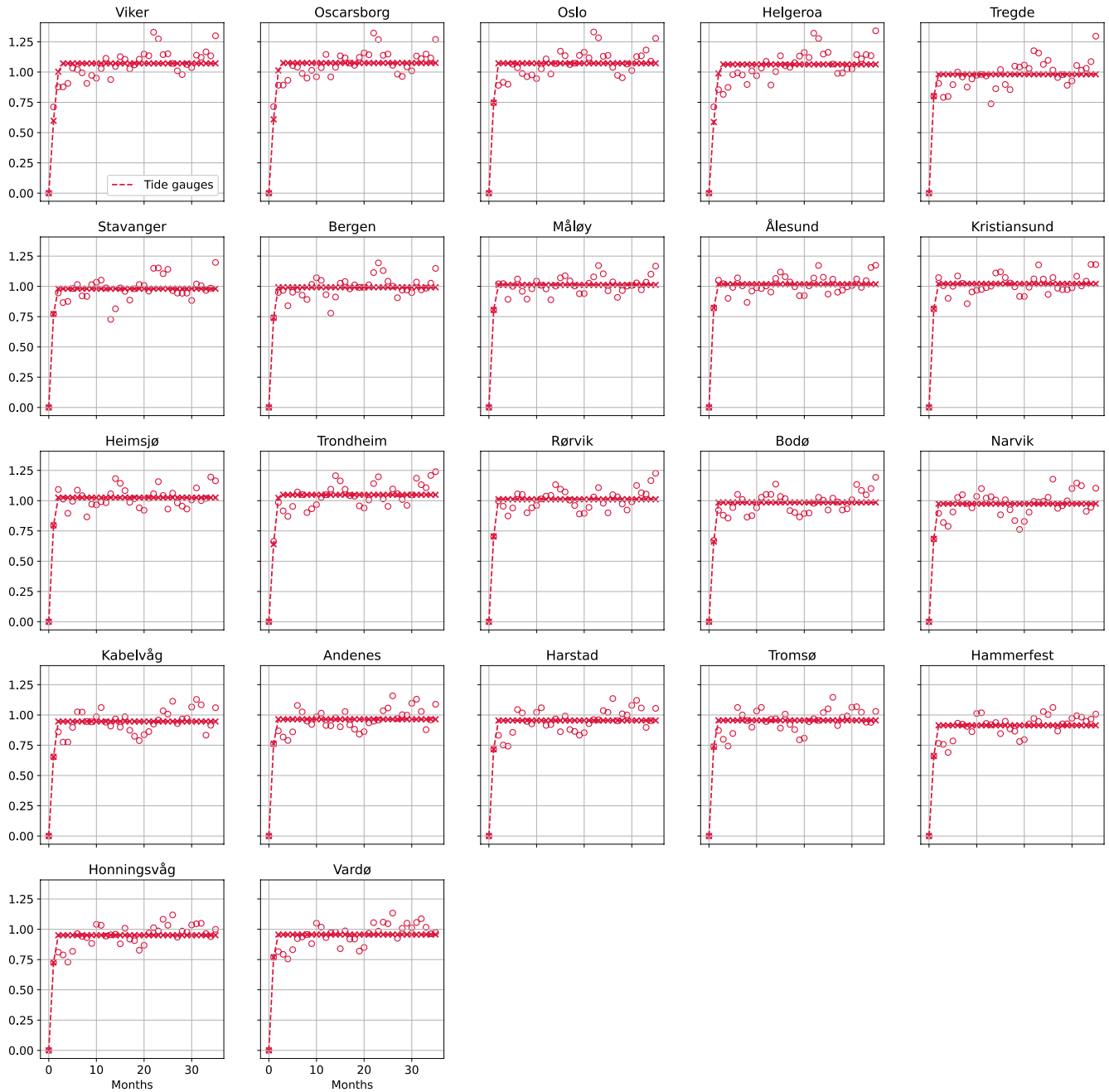
803

804 **Figure A1: For each tide gauge along the Norwegian coast, semi-variogram of the difference between the detrended and deseasoned**
 805 **SLA estimated from the ALES-retracker satellite altimetry (empty circles) and corresponding fit (crosses connected by a dashed line).**
 806 **At each tide gauge location, we scaled each semi-variogram by the variance of the corresponding detrended and deseasoned SLA for**
 807 **all the plots to have the same limits on the y axis.**

808

809

810



811

812

813

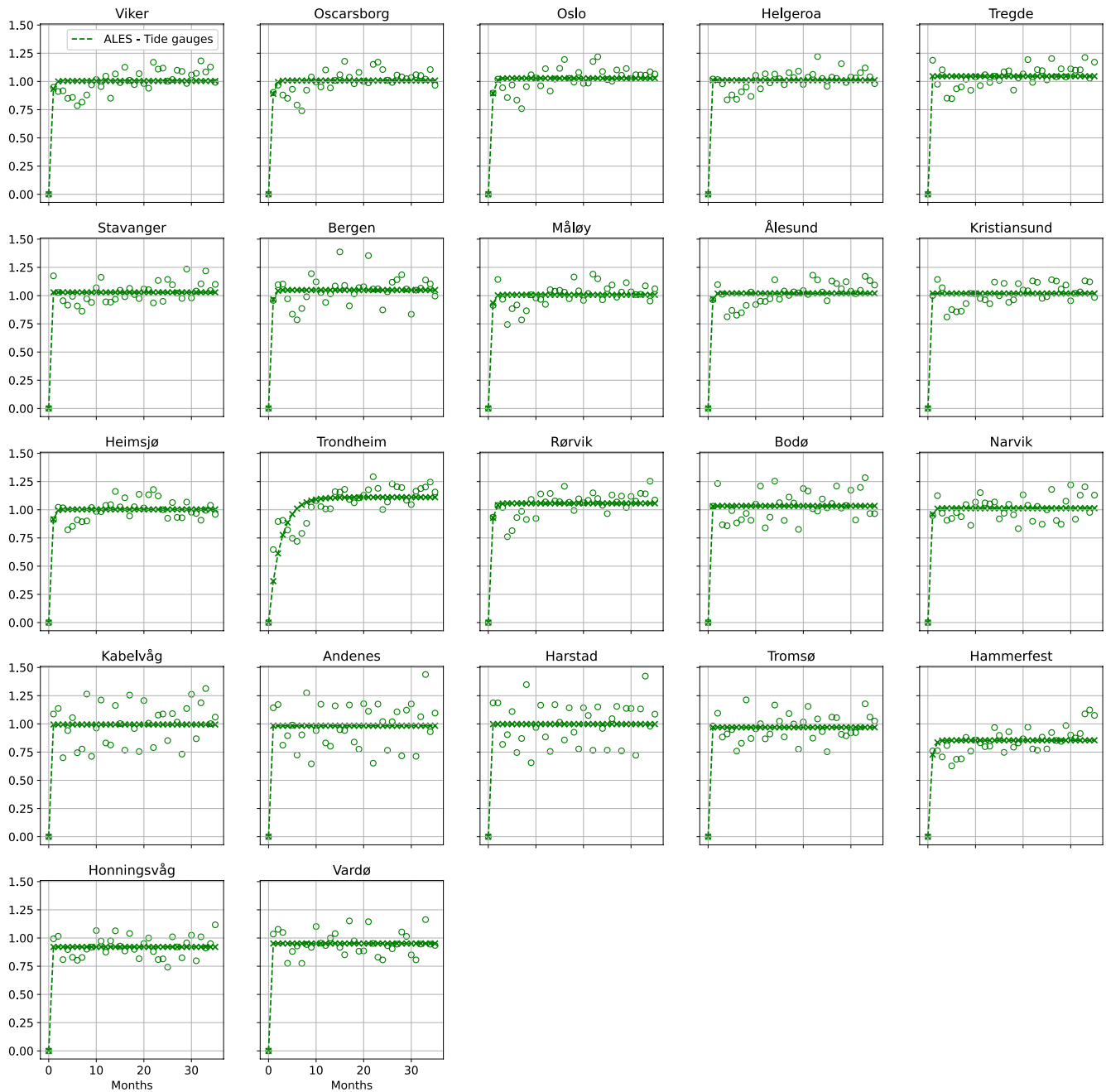
Figure A2: For each tide gauge along the Norwegian coast, semi-variogram of the difference between the detrended and deseasoned SLA measured by the tide gauge (empty circles) and corresponding fit (crosses connected by a dashed line). At each tide gauge

814 location, we scaled each semi-variogram by the variance of the corresponding detrended and deseasoned SLA for all the plots to have
815 the same limits on the y axis.

816

817

818



819

820 **Figure A3:** For each tide gauge along the Norwegian coast, semi-variogram of the difference between the detrended and deseasoned
 821 SLA estimated from the ALES-retracker satellite altimetry and the tide gauge (empty circles) and corresponding fit (crosses connected
 822 by a dashed line). At each tide gauge location, we scaled each semi-variogram by the variance of the corresponding detrended and
 823 deseasoned SLA for all the plots to have the same limits on the y axis.

824

825

826 **Appendix B**

827

828 Following the same argument as in the Appendix A of the Supplementary Material, to estimate the uncertainty
829 associated with the linear trends of the thermosteric, of the halosteric and of the steric components of the sea-
830 level along the Norwegian coast (Fig. 12), we need to account for the effective degrees of freedom in the
831 corresponding time series.

832

833 As in Section A of the Supplementary Material, to determine the effective number of degrees of freedom, we
834 first produce the semi-variograms of the detrended and deseasoned thermosteric, of the halosteric and of the
835 steric components of the sea-level at each hydrographic station. Then, we determine the time needed by the
836 semi-variogram's fit to approximately reach a plateau, adopting an exponential function (See Appendix A).

837

838 The thermosteric sea-level (Fig. B1) shows the strongest serial correlation. The semi-variogram of the
839 thermosteric sea-level returns lags ranging from 3 months, at Indre Utsira, to around 20 months at Skrova. In
840 general, the thermosteric component of the sea-level in northern Norway has fewer degrees of freedom than in
841 the south.

842

843 The halosteric (Fig. B2) and the steric (Fig B3) components show a similar pattern, with the number of effective
844 degrees of freedom being smaller in the north than in the south. However, both components show a weaker
845 serial correlation when compared to the thermosteric component of the sea-level. Indeed, the semi-variograms
846 return lags between 3 and 9 months for both components of the sea-level.

847

848 Similarly to the Appendix A, we use formula (7) ~~the following formula~~ to compute the 95% confidence interval
849 of the linear trend of the SLA and of the thermosteric, halosteric and steric components of the sea-level at each
850 hydrographic station. With respect to (7) though, here we only consider $N^* - 2$ degrees of freedom since the
851 linear model that we use to fit the time series has only two parameters (the offset and the angular coefficient of
852 the straight line).

853

854

$$CI = t_{0.05/2, N^* - 2} \cdot \frac{\sqrt{N-1}}{\sqrt{N^* - 1}} \cdot SE$$

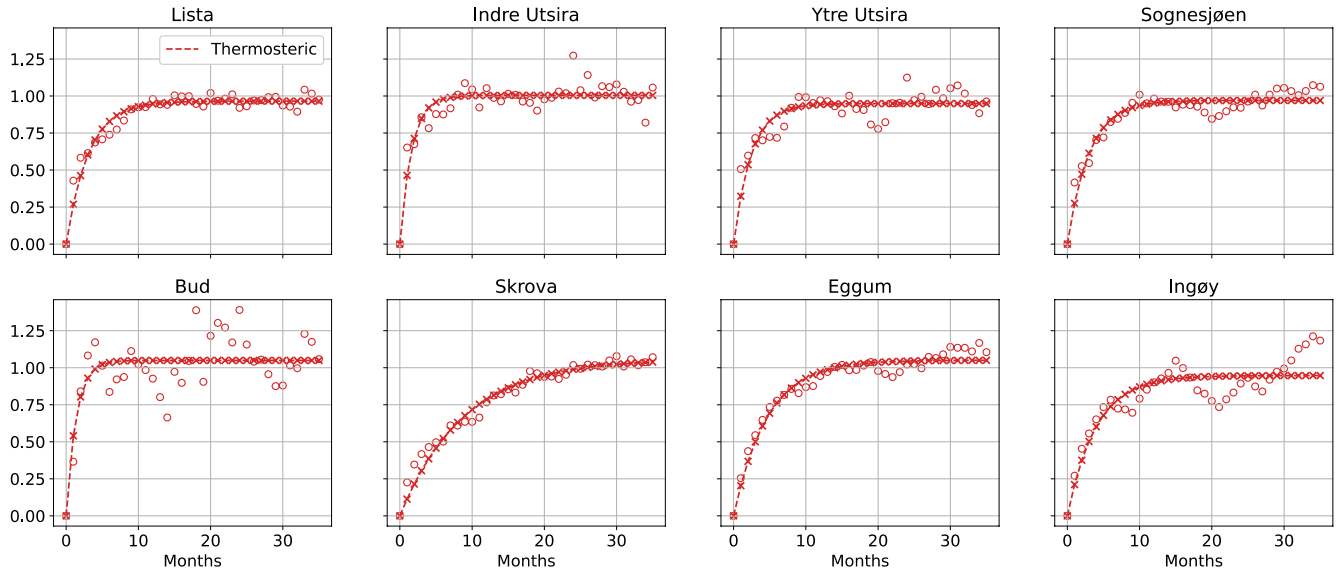
855

856 where SE is the standard error of the linear trend, computed as if $N^* = N$, the total number of observations in

857 the time series, and $t_{0.05/2, N^* - 2}$ is the t values computed using $N^* - 2$ degrees of freedom at a 0.05

858 significance level.

859



860

861 **Figure B1: For each hydrographic station along the Norwegian coast, semi-variogram of the detrended and deseasoned thermosteric**

862 **component of the sea-level variability (empty circles) and corresponding fit (crosses connected by a dashed line). At each**

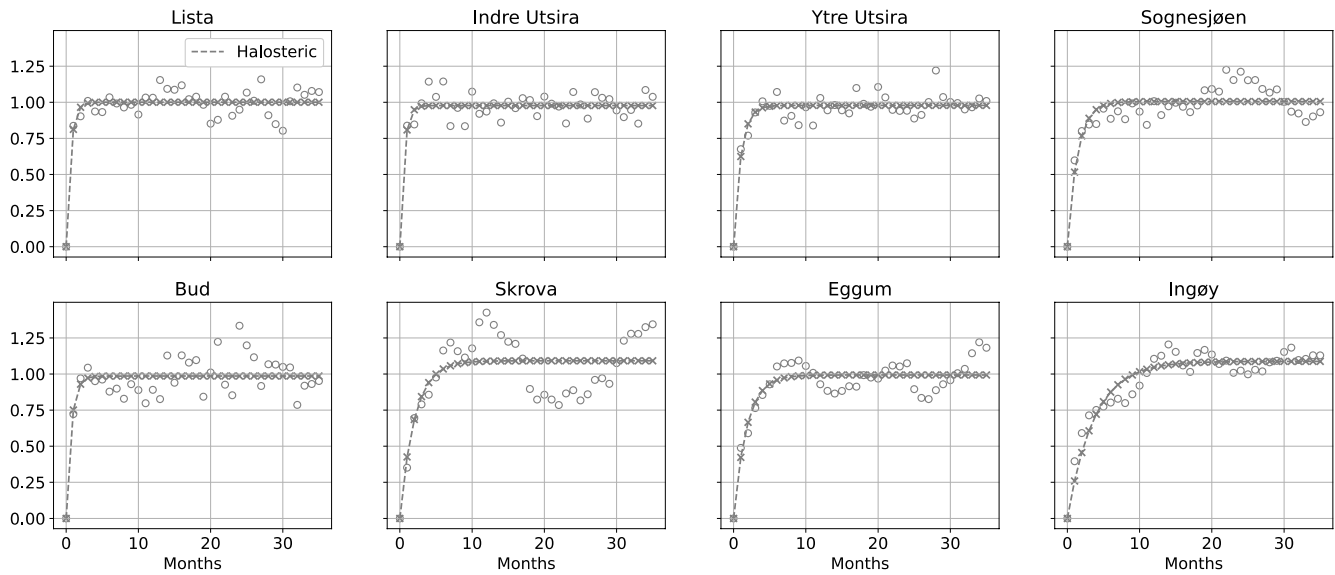
863 **hydrographic station location, we scaled each semi-variogram by the variance of the corresponding detrended and deseasoned**

864 **thermosteric component of the sea-level for all the plots to have the same limits on the y axis.**

865

866

867



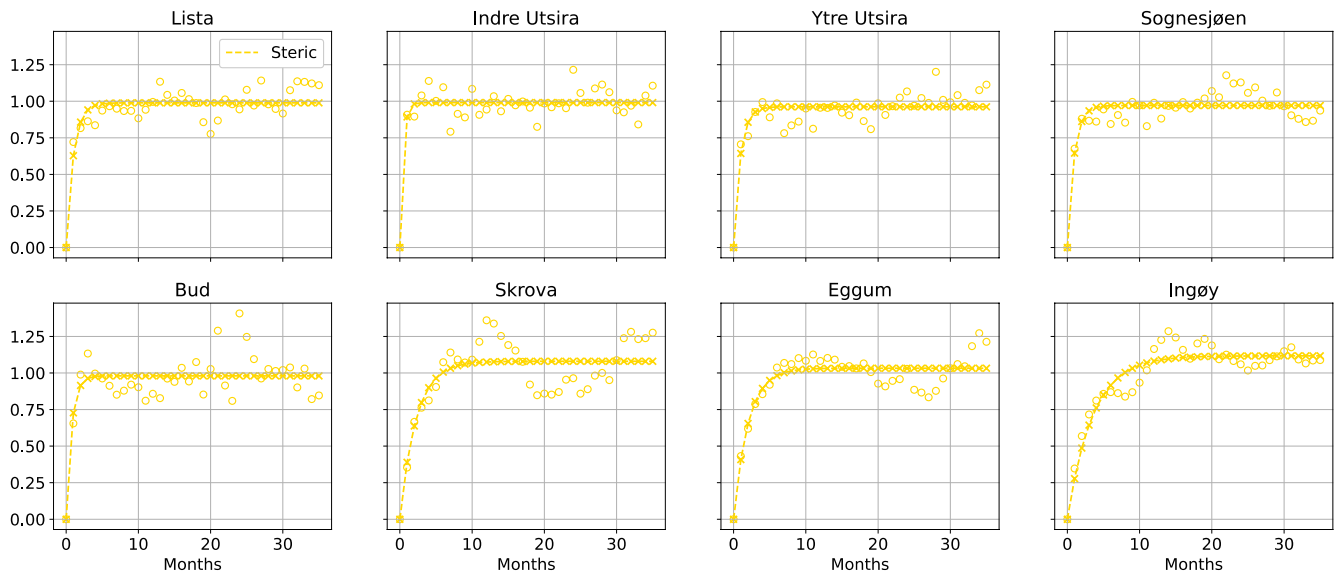
868

869 **Figure B2: For each hydrographic station along the Norwegian coast, semi-variogram of the detrended and deseasoned halosteric**
 870 **component of the sea-level variability (empty circles) and corresponding fit (crosses connected by a dashed line). At each**
 871 **hydrographic station location, we scaled each semi-variogram by the variance of the corresponding detrended and deseasoned**
 872 **halosteric component of the sea-level for all the plots to have the same limits on the y axis.**

873

874

875



876

877 **Figure B3: For each hydrographic station along the Norwegian coast, semi-variogram of the detrended and deseasoned steric**
 878 **component of the sea-level variability (empty circles) and corresponding fit (crosses connected by a dashed line). At each**

879 hydrographic station location, we scaled each semi-variogram by the variance of the corresponding detrended and deseasoned steric
880 component of the sea-level for all the plots to have the same limits on the y axis.

881
882

883 **Appendix C**

884

885 To compare the performance of the ALES-retracked and the conventional satellite altimetry dataset, we have
886 download the along-track L3 satellite altimetry missions provided on the Copernicus website:

887

888 <https://resources.marine.copernicus.eu/product->

889 [download/SEALEVEL_GLO_PHY_L3_REP_OBSERVATIONS_008_062](https://resources.marine.copernicus.eu/product-download/SEALEVEL_GLO_PHY_L3_REP_OBSERVATIONS_008_062).

890

891 even though we should remember that the discrepancy between the two datasets might not only result from
892 the different retrackerers, but also from the different geophysical corrections applied to the data.

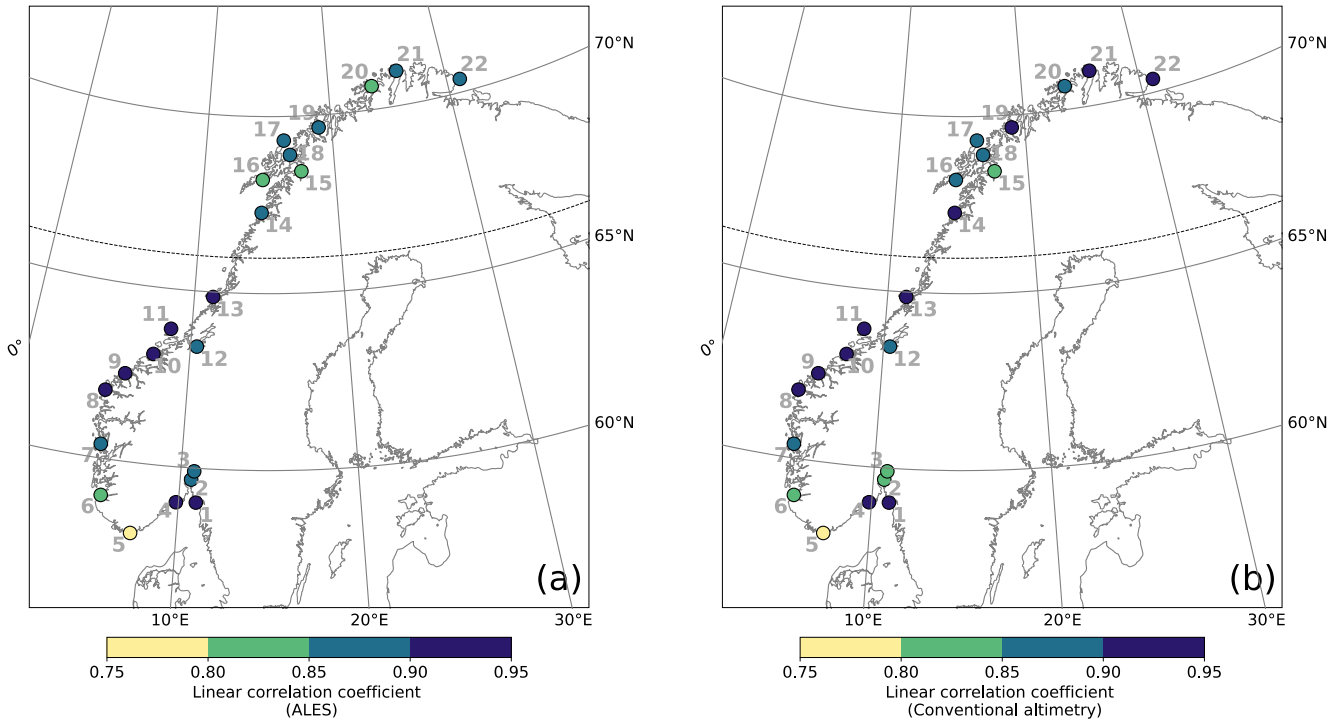
893

894

895 We select the same satellite altimetry missions that have been reprocessed with the ALES-retracker. Moreover,
896 and we make sure that both satellite altimetry datasets cover the same period.

897

1 - Viker	4 - Helgeroa	7 - Bergen	10 - Kristiansund	13 - Rørvik	16 - Kabelvåg	19 - Tromsø	21 - Honningsvåg
2 - Oscarsborg	5 - Tregde	8 - Måløy	11 - Heimsjø	14 - Bodø	17 - Andenes	20 - Hammerfest	22 - Vardø
3 - Oslo	6 - Stavanger	9 - Ålesund	12 - Trondheim	15 - Narvik	18 - Harstad		

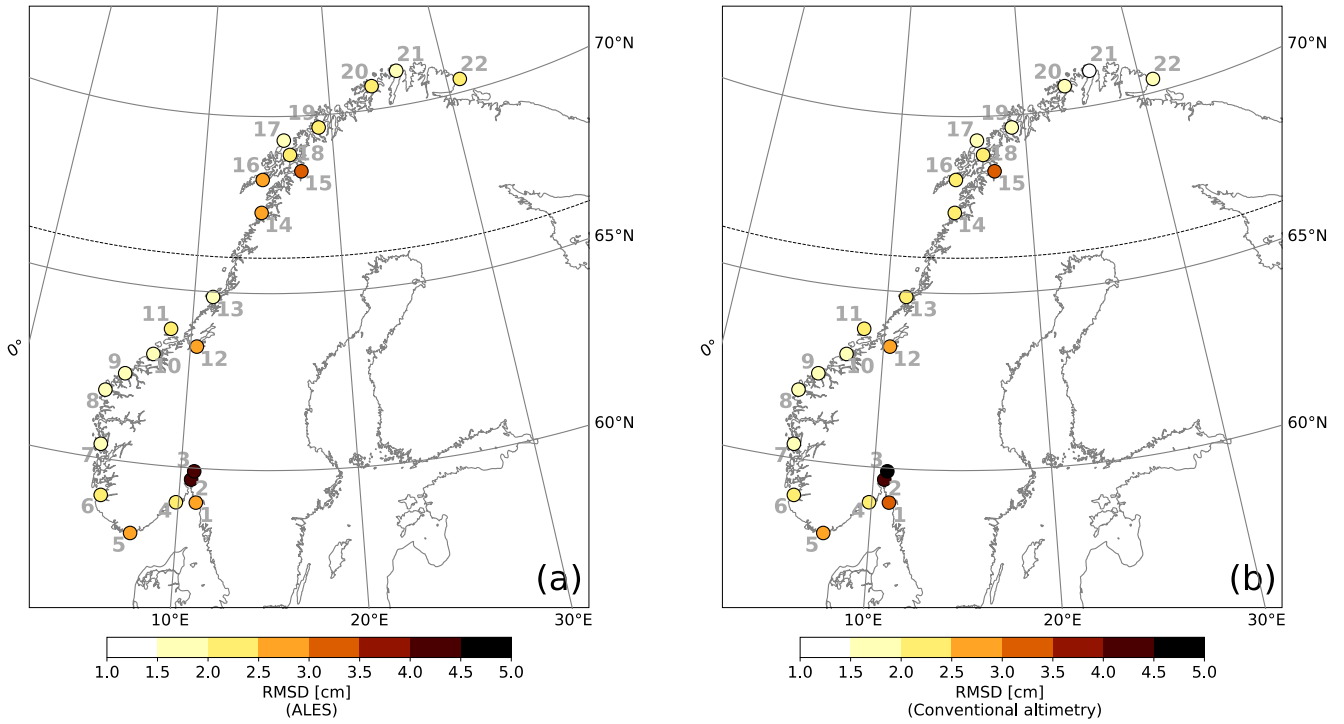


898

899 **Figure C1: Comparison between coastal sea-level signals from in situ measurements and the area-averaged ALES-reprocessed satellite**
900 **altimetry dataset and the conventional satellite altimetry dataset. At each tide gauge location, linear correlation coefficient between the detrended and deseasoned monthly mean SLA from the ALES-reprocessed satellite altimetry dataset and from the tide gauge (a),**
901 **and from the conventional altimetry dataset and the tide gauge. The black, dashed line indicates the 66°N parallel.**
902
903

904

1 - Viker	4 - Helgeroa	7 - Bergen	10 - Kristiansund	13 - Rørvik	16 - Kabelvåg	19 - Tromsø	21 - Honningsvåg
2 - Oscarsborg	5 - Tregde	8 - Måløy	11 - Heimsjø	14 - Bodø	17 - Andenes	20 - Hammerfest	22 - Vardø
3 - Oslo	6 - Stavanger	9 - Ålesund	12 - Trondheim	15 - Narvik	18 - Harstad		



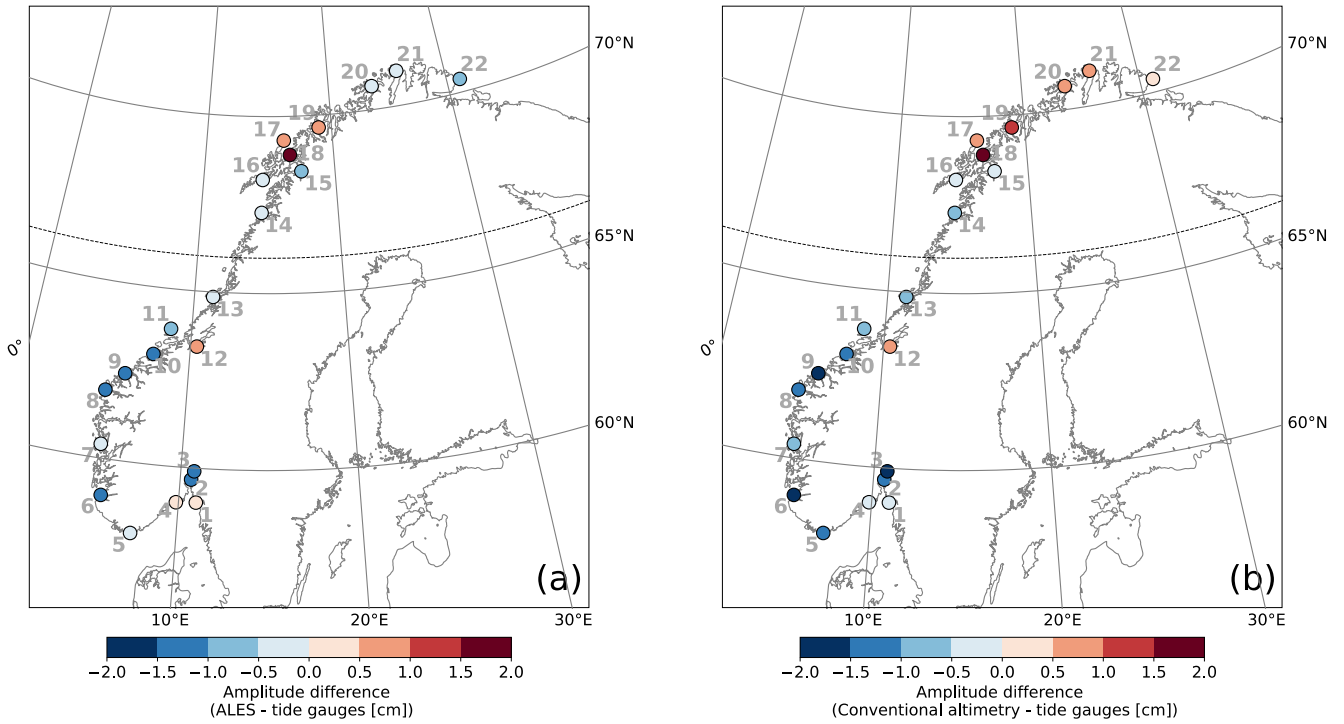
905

906 **Figure C2: Comparison between coastal sea-level signals from in situ measurements and the area-averaged ALES-reprocessed satellite**
 907 **altimetry dataset and the conventional satellite altimetry dataset. At each tide gauge location, RMSD of the detrended and**
 908 **deseasoned monthly mean SLA from the ALES-reprocessed satellite altimetry dataset and from the tide gauge (a), and from the**
 909 **conventional altimetry dataset and the tide gauge. The black, dashed line indicates the 66°N parallel.**

910

911

1 - Viker	4 - Helgeroa	7 - Bergen	10 - Kristiansund	13 - Rørvik	16 - Kabelvåg	19 - Tromsø	21 - Honningsvåg
2 - Oscarsborg	5 - Tregde	8 - Måløy	11 - Heimsjø	14 - Bodø	17 - Andenes	20 - Hammerfest	22 - Vardø
3 - Oslo	6 - Stavanger	9 - Ålesund	12 - Trondheim	15 - Narvik	18 - Harstad		



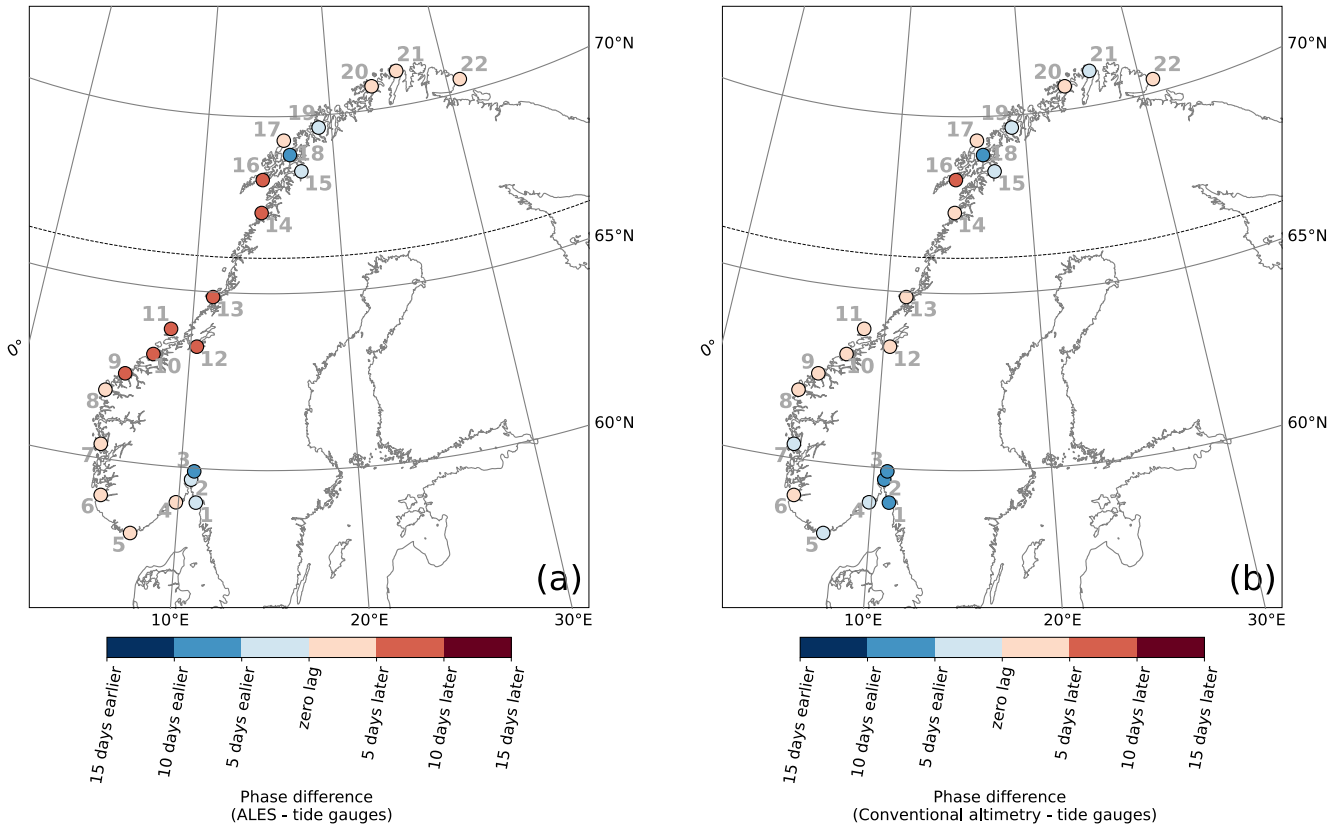
912

913 **Figure C3: Comparison between coastal sea-level signals from in situ measurements and the area-averaged ALES-reprocessed satellite**
 914 **altimetry dataset and the conventional satellite altimetry dataset. At each tide gauge location, difference between the amplitude of**
 915 **the annual cycle from the ALES-reprocessed altimetry dataset and the tide gauge (a), and from the conventional altimetry dataset and**
 916 **the tide gauge (b). The black, dashed line indicates the 66°N parallel.**
 917

918

919

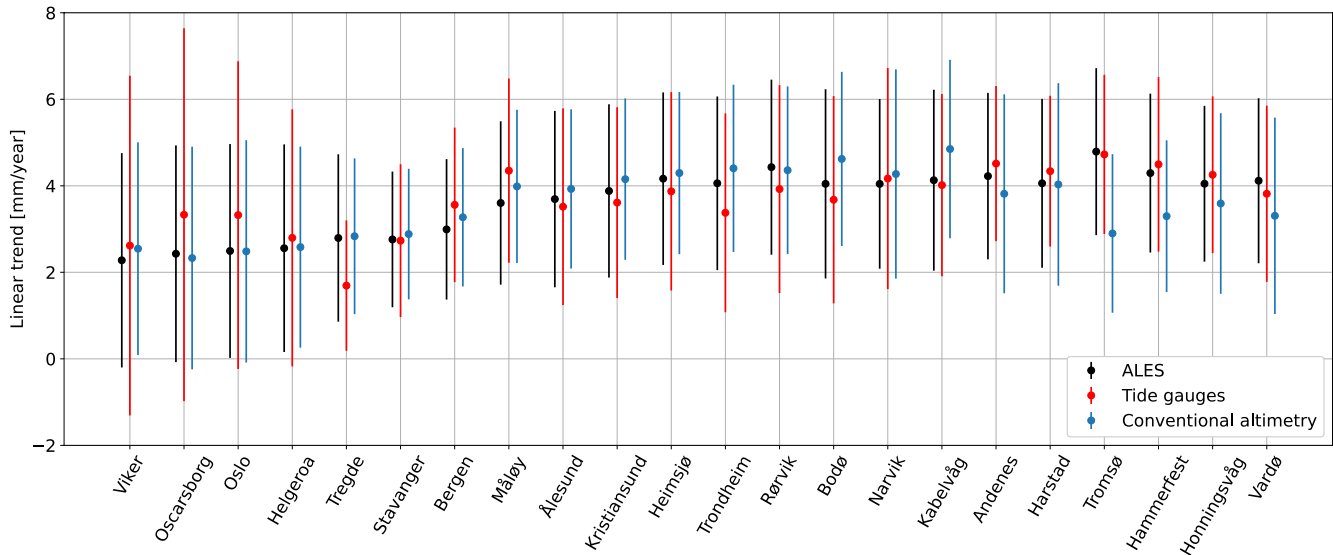
1 - Viker	4 - Helgeroa	7 - Bergen	10 - Kristiansund	13 - Rørvik	16 - Kabelvåg	19 - Tromsø	21 - Honningsvåg
2 - Oscarsborg	5 - Tregde	8 - Måløy	11 - Heimsjø	14 - Bodø	17 - Andenes	20 - Hammerfest	22 - Vardø
3 - Oslo	6 - Stavanger	9 - Ålesund	12 - Trondheim	15 - Narvik	18 - Harstad		



920

921 **Figure C4: Comparison between coastal sea-level signals from in situ measurements and the area-averaged ALES-reprocessed satellite**
 922 **altimetry dataset and the conventional satellite altimetry dataset. At each tide gauge location, difference between the phase of the**
 923 **annual cycle from the ALES-reprocessed altimetry dataset and the tide gauge (a), and from the conventional altimetry dataset and the**
 924 **tide gauge (b). The black, dashed line indicates the 66°N parallel.**

925



926
927
928
929
930

Figure C5: At each tide gauge location, linear trend of the SLA from the ALES-reprocessed altimetry dataset (black dots), from conventional altimetry dataset (cyan dots) and from tide gauges (red dots). The error bars show the 95th confidence intervals of the sea-level trend at each tide gauge location.

931
932

933 **Data availability**

934 The tide gauge data are available and distributed through a dedicated web API (api.sehavniva.no). The ALES-
935 reprocessed satellite altimetry dataset is available at the Open Altimetry Database website of the Technische
936 Universität München (<https://openadb.dgfi.tum.de/en/>). The hydrographic stations dataset are updated and
937 available at <http://www.imr.no/forskning/forskningsdata/stasjoner/index.html>. The NCEP/NCAR v2 dataset is
938 available at <https://psl.noaa.gov/data/gridded/data.ncep.reanalysis2.html>.

939

940 **Author contribution**

941 FM, AB, LC and LB designed the research study. JEØN removed the geophysical signal from the sea-level
942 measured by the tide gauges. FM wrote the code to analyse the data. All authors contributed to the analysis of
943 the results, and to the writing and the editing of the paper.

944

945 **Competing interests**

946 The authors declare that they have no conflict of interest.

947

948 **Acknowledgements**

949 We would like to thank the two reviewers who significantly helped improved this manuscript. All products are
950 computed based on altimetry missions operated by NASA/CNES (TOPEX, Jason-1), ESA (ERS-1/2, Envisat,
951 Cryosat-2), USNavy/NOAA (GFO), CNES/NASA/Eumetsat/NOAA (Jason-2, Jason-3), ISRO/CNES (SARAL), and
952 ~~EUMETSAT (Sentinel-3)~~. The original data sets are disseminated by AVISO, ESA, NOAA, and PODAAC. Michael
953 Hart-Davis (TUM) is kindly acknowledged for providing the EOT11a tidal model data, and Kristian Breili
954 (Norwegian Mapping Authority) for providing the GIA data. Léon Chafik acknowledges support from the
955 Swedish National Space Agency (Dnr: 133/17, 204/19).

956

957

958

959

960 **References**

961 Abulaitijiang, A., Andersen, O. B., and Stenseng, L.: Coastal sea level from inland CryoSat-2 interferometric SAR
962 altimetry, *Geophys. Res. Lett.*, 42, 1841-1847, <https://doi.org/10.1002/2015GL063131>, 2015.

963

964 Bartlett, M. S.: Some Aspects of the Time-Correlation Problem in Regard to Tests of Significance, *J. R. Stat. Soc.*,
965 98, 536-543, <https://doi.org/10.2307/2342284>, 1935.

966

967 Benveniste, J., Birol, F., Calafat, F., Cazenave, A., Dieng, H., Gouzenes, Y., Legeais, J. F., Léger, F., Niño, F.,
968 Passaro, M., Schwatke, C., and Shaw, A.: Coastal sea level anomalies and associated trends from Jason satellite
969 altimetry over 2002-2018, *Sci. Data*, 7, 1–17, <https://doi.org/10.1038/s41597-020-00694-w>, 2020.

970

971 Bonaduce, A., Pinardi, N., Oddo, P., Spada, G., and Larnicol, G.: Sea-level variability in the Mediterranean Sea
972 from altimetry and tide gauges, *Clim. Dyn.*, 47, 2851-2866, <https://doi.org/10.1007/s00382-016-3001-2>, 2016.

973

974 Breili, K., Simpson, M. J. R., and Nilsen, J. E. Ø.: Observed sea-level changes along the Norwegian coast, *J. Mar.*
975 *Sci. Eng.*, 5, 1-19, <https://doi.org/10.3390/jmse5030029>, 2017.

976

977 Carrère, L. and Lyard, F.: Modeling the barotropic response of the global ocean to atmospheric wind and
978 pressure forcing - Comparisons with observations, *Geophys. Res. Lett.*, 30,
979 <https://doi.org/10.1029/2002GL016473>, 2003.

980

981 Cazenave, A., Palanisamy, H., and Ablain, M.: Contemporary sea level changes from satellite altimetry: What
982 have we learned? What are the new challenges?, *Adv. Space Res.*, 62, 1639-1653,
983 <https://doi.org/10.1016/j.asr.2018.07.017>, 2018.
984

985 Chafik, L., Nilsson, J., Skagseth, and Lundberg, P.: On the flow of Atlantic water and temperature anomalies in
986 the Nordic Seas toward the Arctic Ocean, *J. Geophys. Res. Oceans*, 120, 7897-7918,
987 <https://doi.org/10.1002/2015JC011012>, 2015.
988

989 Chafik, L., Nilsen, J. E. Ø., and Dangendorf, S.: Impact of North Atlantic teleconnection patterns on northern
990 European sea level, *J. Mar. Sci. Eng.*, 5, 1-23, <https://doi.org/10.3390/jmse5030043>, 2017.
991

992 Chafik, L., Nilsen, J. E. Ø., Dangendorf, S., Reverdin, G., and Frederikse, T.: North Atlantic Ocean Circulation and
993 Decadal Sea Level Change During the Altimetry Era, *Sci. Rep.*, 9, 1-9, [https://doi.org/10.1038/s41598-018-](https://doi.org/10.1038/s41598-018-37603-6)
994 [37603-6](https://doi.org/10.1038/s41598-018-37603-6), 2019.
995

996 Cipollini, P., Benveniste, J., Bouffard, J., Emery, W., Fenoglio-Marc, L., Gommenginger, C., Griffin, D., Høyer, J.,
997 Kuparov, A., Madsen, K., Mercier, F., Miller, L., Pascual, A., Ravichandran, M., Shillington, F., Snaith, H., Sturb, P.,
998 T., Vandemark, D., Vignudelli, S., Wilkin, J., Woodworth, P., and Zavala-Garay, J.: The Role of Altimetry in Coastal
999 Observing Systems. In: Hall J, Harrison DE, Stammer D (eds) *Proceedings of OceanObs'09: sustained ocean*
1000 *observations and information for society*, vol 2. European Space Agency, WPP-306, pp 181–191. (19) (PDF)
1001 *Coastal gravity field refinement by combining airborne and ground-based data*.
1002 <https://doi.org/10.5270/oceanobs09.cwp.16>, 2010.
1003

1004 Cipollini, P., Benveniste, J., Birol, F., Joana Fernandes, M., Obligis, E., Passaro, M., Ted Strub, P., Valladeau, G.,
1005 Vignudelli, S., and Wilkin, J.: Satellite altimetry in coastal regions, in: *Satellite Altimetry Over Oceans and Land*
1006 *Surfaces*, *Surv. Geophys.*, 38, 33-57, <https://doi.org/10.1201/9781315151779>, 2017.
1007

1008 Frederikse, T., Jevrejeva, S., Riva, R. E. M., and Dangendorf, S.: A consistent sea-level reconstruction and its
1009 budget on basin and global scales over 1958-2014, *J. Clim.*, 31, 1267-1280, [https://doi.org/10.1175/JCLI-D-17-](https://doi.org/10.1175/JCLI-D-17-0502.1)
1010 [0502.1](https://doi.org/10.1175/JCLI-D-17-0502.1), 2018.
1011

1012 Frederikse, T., Landerer, F., Caron, L., Adhikari, S., Parkes, D., Humphrey, V. W., Dangendorf, S., Hogarth, P.,
1013 Zanna, L., Cheng, L., and Wu, Y. H.: The causes of sea-level rise since 1900, *Nature*, 584, 393-397,
1014 <https://doi.org/10.1038/s41586-020-2591-3>, 2020.
1015

1016 Gill, A. E. and Niller, P. P.: The theory of the seasonal variability in the ocean, *Deep Sea Res. Oceanogr. Abstr.*,
1017 20, 141-177, [https://doi.org/10.1016/0011-7471\(73\)90049-1](https://doi.org/10.1016/0011-7471(73)90049-1), 1973.
1018

1019 Gómez-Enri, J., Vignudelli, S., Quartly, G. D., Gommenginger, C. P., Cipollini, P., Challenor, P. G., and Benveniste,
1020 J.: Modeling Envisat RA-2 waveforms in the coastal zone: Case study of calm water contamination, *IEEE Geosci.*
1021 *Remote Sensing Lett.*, 7, 474–478, <https://doi.org/10.1109/LGRS.2009.2039193>, 2010.
1022

1023 Hermans, T. H. J., Gregory, J. M., Palmer, M. D., Ringer, M. A., Katsman, C. A., and Slangen, A. B. A.: Projecting
1024 Global Mean Sea-Level Change Using CMIP6 Models, *Geophys. Res. Let.*, 48,
1025 <https://doi.org/10.1029/2020GL092064>, 2021.
1026
1027 Ji, M., Reynolds, R. W., and Behringer, D. W.: Use of TOPEX/Poseidon sea level data for Ocean analyses and
1028 ENSO prediction: Some early results, *J. Clim.*, 13, 216-231, <https://doi.org/10.1175/1520->
1029 [0442\(2000\)013<0216:UOTPSL>2.0.CO;2](https://doi.org/10.1175/1520-0442(2000)013<0216:UOTPSL>2.0.CO;2), 2000.
1030
1031 Lichter, M., Vafeidis, A. T., Nicholls, R. J., and Kaiser, G.: Exploring data-related uncertainties in analyses of land
1032 area and population in the “Low-Elevation Coastal Zone” (LECZ), *J. Coast. Res.*, 27 (4), 757-768,
1033 <https://doi.org/10.2112/JCOASTRES-D-10-00072.1>, 2011.
1034
1035 Liebmann, B., Dole, R. M., Jones, C., Bladé, I., and Allured, D.: Influence of choice of time period on global
1036 surface temperature trend estimates, *Bull. Am. Meteorol. Soc.*, 91, 1485-1491,
1037 <https://doi.org/10.1175/2010BAMS3030.1>, 2010.
1038
1039 Madsen, K. S., Høyer, J. L., Suursaar, Ü., She, J., and Knudsen, P.: Sea Level Trends and Variability of the Baltic
1040 Sea From 2D Statistical Reconstruction and Altimetry, *Front. Earth Sci.*, 7,
1041 <https://doi.org/10.3389/feart.2019.00243>, 2019.
1042
1043 Nerem, R. S., Chambers, D. P., Choe, C., and Mitchum, G. T.: Estimating Mean Sea Level Change from the TOPEX
1044 and Jason Altimeter Missions, *Mar. Geod.*, 33, 435-446, <https://doi.org/10.1080/01490419.2010.491031>, 2010.
1045
1046 Nicholls, R. J.: Planning for the Impacts of Sea Level Rise, *Oceanography*, 24, 144–157, 2011.
1047 Oelsmann, J., Passaro, M., Dettmering, D., Schwatke, C., Sanchez, L., and Seitz, F.: The Zone of Influence:
1048 Matching sea level variability from coastal altimetry and tide gauges for vertical land motion estimation, *Ocean*
1049 *Sci.*, 17, 35-57, <https://doi.org/10.5194/os-2020-29>, 2021.
1050
1051 Passaro, M., Cipollini, P., Vignudelli, S., Quartly, G. D., and Snaith, H. M.: ALES: A multi-mission adaptive
1052 subwaveform retracker for coastal and open ocean altimetry, *Remote Sens. Environ.*, 145, 173-189,
1053 <https://doi.org/10.1016/j.rse.2014.02.008>, 2014.
1054
1055 Passaro, M., Cipollini, P., and Benveniste, J.: Annual sea level variability of the coastal ocean: The Baltic Sea-
1056 North Sea transition zone, *J. Geophys. Res. Oceans*, 120, 3061-3078, <https://doi.org/10.1002/2014JC010510>,
1057 2015.
1058
1059 Passaro, M., Dinardo, S., Quartly, G. D., Snaith, H. M., Benveniste, J., Cipollini, P., and Lucas, B.: Cross-calibrating
1060 ALES Envisat and CryoSat-2 Delay-Doppler: A coastal altimetry study in the Indonesian Seas, *Adv. Space Res.*, 58,
1061 289-303, <https://doi.org/10.1016/j.asr.2016.04.011>, 2016.
1062
1063 Passaro, M., Rose, S. K., Andersen, O. B., Boergens, E., Calafat, F. M., Dettmering, D., and Benveniste, J.: ALES+:
1064 Adapting a homogenous ocean retracker for satellite altimetry to sea ice leads, coastal and inland waters,
1065 *Remote Sens. Environ.*, 211, 456-471, <https://doi.org/10.1016/j.rse.2018.02.074>, 2018.

1066
1067 Passaro, M., Müller, F. L., Oelmann, J., Rautiainen, L., Dettmering, D., Hart-Davis, M. G., Abulaitijiang, A.,
1068 Andersen, O. B., Høyer, J. L., Madsen, K. S., Ringgaard, I. M., Särkkä, J., Scarratt, R., Schwatke, C., Seitz, F.,
1069 Tuomi, L., Restano, M., and Benveniste, J.: Absolute Baltic Sea Level Trends in the Satellite Altimetry Era: A
1070 Revisit, *Front. Mar. Sci.*, 8, <https://doi.org/10.3389/fmars.2021.647607>, 2021.
1071
1072 Picaut, J., Hackert, E., Busalacchi, A. J., Murtugudde, R., and Lagerloef, G. S. E.: Mechanisms of the 1997–1998 El
1073 Niño–La Niña, as inferred from space-based observations, *J. Geophys. Res.*, 107,
1074 <https://doi.org/10.1029/2001jc000850>, 2002.
1075
1076 Raj, R. P., Andersen, O. B., Johannessen, J. A., Gutknecht, B. D., Chatterjee, S., Rose, S. K., Bonaduce, A.,
1077 Horwath, M., Ranndal, H., Richter, K., Palanisamy, H., Ludwigsen, C. A., Bertino, L., Nilsen, J. E. Ø., Knudsen, P.,
1078 Hogg, A., Cazenave, A., and Benveniste, J.: Arctic sea level budget assessment during the grace/argo time
1079 period, *Remote Sens.*, 12, <https://doi.org/10.3390/rs12172837>, 2020.
1080
1081 Richter, K., Nilsen, J. E. Ø., and Drange, H.: Contributions to sea level variability along the Norwegian coast for
1082 1960–2010, *J. Geophys. Res.*, 117, <https://doi.org/10.1029/2011JC007826>, 2012.
1083
1084 Richter, K., Meyssignac, B., Slangen, A. B. A., Melet, A., Church, J. A., Fettweis, X., Marzeion, B., Agosta, C.,
1085 Ligtenberg, S. R. M., Spada, G., Palmer, M. D., Roberts, C. D., and Champollion, N.: Detecting a forced signal in
1086 satellite-era sea-level change, *Environ. Res. Lett.*, 15, <https://doi.org/10.1088/1748-9326/ab986e>, 2020.
1087
1088 Rose, S. K., Andersen, O. B., Passaro, M., Ludwigsen, C. A., and Schwatke, C.: Arctic ocean sea level record from
1089 the complete radar altimetry era: 1991–2018, *Remote Sens.*, 11, <https://doi.org/10.3390/rs11141672>, 2019.
1090
1091 Siegmund, F., Johannessen, J., Drange, H., Mork, K. A., and Korabely, A.: Steric height variability in the Nordic
1092 Seas, *J. Geophys. Res.*, 112, <https://doi.org/10.1029/2007JC004221>, 2007.
1093
1094 Simpson, M. J. R., Nilsen, J. E. Ø., Ravndal, O. R., Breili, K., Sande, H., Kierulf, H. P., Steffen, H., Jansen, E., Carson,
1095 M., and Vestøl, O.: Sea Level Change for Norway Past and Present Observations and Projections to 2100, 1–156
1096 pp., 2015.
1097
1098 Simpson, M. J. R., Ravndal, O. R., Sande, H., Nilsen, J. E. Ø., Kierulf, H. P., Vestøl, O., and Steffen, H.: Projected
1099 21st century sea-level changes, observed sea level extremes, and sea level allowances for Norway, *J. Mar. Sci.*
1100 *Eng.*, 5, <https://doi.org/10.3390/jmse5030036>, 2017.
1101
1102 Stammer, D., Cazenave, A., Ponte, R. M., and Tamisiea, M. E.: Causes for contemporary regional sea level
1103 changes, *Annu. Rev. Mar. Sci.*, 5, 21–46, <https://doi.org/10.1146/annurev-marine-121211-172406>, 2013.
1104
1105 Volkov, D. L. and Pujol, M. I.: Quality assessment of a satellite altimetry data product in the Nordic, Barents, and
1106 Kara seas, *J. Geophys. Res.*, 117, <https://doi.org/10.1029/2011JC007557>, 2012.
1107
1108 Wackernagel, H.: *Multivariate Geostatistics*, 3rd ed., Springer, Berlin, Heidelberg, 1–388 pp., 2003.

1109

1110 Woodworth, P. L.: A note on the nodal tide in sea level records, *J. Coastal Res.*, 28 (2), 316-323,

1111 <https://doi.org/10.2112/JCOASTRES-D-11A-00023.1>, 2012.

1112

1113 Xu, X.-Y., Xu, K., Xu, Y., and Shi, L.-W.: Coastal Altimetry: A Promising Technology for the Coastal Oceanography

1114 Community, in: *Estuaries and Coastal Zones - Dynamics and Response to Environmental Changes*, *Surv.*

1115 *Geophys.*, 40, 1351-1397, <https://doi.org/10.5772/intechopen.89373>, 2019.

1116

1117 Zhang, Z., Lu, Y., and Hsu, H.: Detecting ocean currents from satellite altimetry, satellite gravity and ocean data,

1118 in *Dynamic Planet*, International Association of Geodesy Symposia, edited by P. Tregoning, and C. Rizos,

1119 Springer, Berlin.

1120 https://doi.org/10.1007/978-3-540-49350-1_3, 2007.

1121

1122

1123

1124